A dual function of the IDA peptide in regulating cell separation and modulating plant immunity at the molecular level

Vilde Olsson Lalun[1], Maike Breiden[§2], Sergio Galindo-Trigo[1§], Elwira Smakowska-Luzan[3], Rüdiger Simon[2] and Melinka A. Butenko[1*]

[1]Section for Genetics and Evolutionary Biology, Department of Biosciences, University of Oslo, 0316 Oslo, Norway

[2]Institute for Developmental Genetics and Cluster of Excellence on Plant Sciences, Heinrich Heine University, Universitätsstraße 1, 40225 Düsseldorf, Germany

[3]Gregor Mendel Institute (GMI), Austrian Academy of Sciences, Vienna Biocenter (VBC), Dr Bohr-Gasse 3, 1030 Vienna, Austria

[§]Equal contribution

*Corresponding author; email: m.a.butenko@ibv.uio.no

Abstract:

The abscission of floral organs and emergence of lateral roots in Arabidopsis is regulated by the peptide ligand INFLORESCENCE DEFICIENT IN ABSCISSION (IDA) and the receptor protein kinases HAESA (HAE) and HAESA-LIKE 2 (HSL2). During these cell separation processes, the plant induces defense-associated genes to protect against pathogen invasion. However, the molecular coordination between abscission and immunity has not been thoroughly explored. Here we show that IDA induces a release of cytosolic calcium ions (Ca^{2+}) and apoplastic production of reactive oxygen species, which are signatures of early defense responses. In addition, we find that IDA promotes late defense responses by the transcriptional upregulation of genes known to be involved in immunity. When comparing the IDA induced early immune responses to known immune responses, such as those elicited by flagellin22 treatment, we observe both similarities and differences. We propose a molecular mechanism by which IDA promotes signatures of an immune response in cells destined for separation to guard them from pathogen attack.

Introduction

All multicellular organisms require tightly regulated cell-to-cell communication during development and adaptive responses. In addition to hormones, plants use small-secreted peptide ligands to regulate these highly coordinated events of growth, development and responses to abiotic and biotic stress (Matsubayashi, 2011; Olsson et al., 2018). In plants, organ separation or abscission, involves cell separation between specialized abscission zone (AZ) cells and enables the removal of unwanted or diseased organs in response to endogenous developmental signals or environmental stimuli. *Arabidopsis thaliana* (Arabidopsis) abscise floral organs (stamen, petals and sepals) after pollination, and this system has been used as a model to study the regulation of cell separation and abscission (Bleecker & Patterson, 1997). Precise cell separation also occurs during the emergence of new lateral root (LR) primordia, root cap sloughing, formation of stomata and radicle emergence during germination (Roberts et al., 2000). In Arabidopsis, the INFLORESCENCE DEFICIENT IN ABSCISSION (IDA) peptide mediated signaling system ensures the correct spatial and temporal abscission of sepals, petals, and stamens. The IDA protein shares a conserved C-terminal domain with the other 7 IDA-LIKE (IDL) members (Butenko et al., 2003, Vie et al., 2015) which is processed to a functional 12 amino acid hydroxylated peptide (Butenko et al., 2014). The abscission process is regulated by the production and release of IDA, which binds the genetically redundant plasma membrane (PM) localized receptor kinases (RKs), HAESA (HAE) and HAESA-LIKE 2 (HSL2). IDA binding to HAE and HSL2 promotes receptor association with members of the co-receptor SOMATIC EMBRYOGENESIS RECEPTOR KINASE (SERK) family and further downstream signaling leading to cell separation events. (Cho et al., 2008; Meng et al., 2016; Santiago et al., 2016; Stenvik et al., 2008). Recently, it has been shown that IDA and IDL family members also bind and activate HSL1 in the regulation of leaf epidermal pattering, indicating subfunctionalisation within this clade of receptors (Roman et al., 2022) and opens for the possibility that HAE or HSL2 could have additional functions than regulating cell separation events.

A deficiency in the IDA signaling pathway prevents the expression of genes encoding secreted cell wall remodeling and hydrolase enzymes thus hindering floral organs to abscise (Butenko et al., 2003; Cho et al., 2008; Kumpf et al., 2013; Xiangzong Meng et al., 2016; Niederhuth et al., 2013; Stenvik et al., 2008; Isaiah Taylor & John C. Walker, 2018). Interestingly, components of the IDA signaling pathway control different cell separation events during Arabidopsis development. IDA signaling through HAE and HSL2 regulates cell wall remodeling genes in the endodermal, cortical, and epidermal tissues overlaying the LR primordia during LR emergence (Kumpf et al., 2013). In addition, IDL1 signals through HSL2 to regulate cell separation during root cap sloughing (Shi et al., 2018).

Plant cell walls act as physical barriers against pathogenic invaders. The cell-wall processing and remodeling that occurs during abscission leads to exposure of previously protected tissue. This provides an entry point for phytopathogens thereby increasing the need for an effective defense system in these

cells (Agustí et al., 2009). Indeed, it has been shown that AZ cells undergoing cell separation express defense genes and it has been proposed that they function in protecting the AZ from infection after abscission has occurred (Cai & Lashbrook, 2008; Niederhuth et al., 2013). IDA elicits the production of Reactive Oxygen Species (ROS) in *Nicotiana benthamiana* (*N.benthamiana*) leaves transiently expressing the HAE or HSL2 receptor (Butenko et al., 2014). As a consequence of defense responses, ROS occurs in the apoplast and is involved in regulating the cell wall structure by producing cross-linking of cell wall components in the form of hydrogen peroxide (H_2O_2) or act as cell wall loosening agents in the form of hydroxyl radical ($^{\cdot}OH$)radicals (Kärkönen & Kuchitsu, 2015). ROS may also serve as a direct defense response by their highly reactive and toxic properties (Kärkönen & Kuchitsu, 2015). In addition, ROS may act as a secondary signaling molecule enhancing intracellular defense responses as well as contributing to the induction of defense related genes (Reviewed in (Castro et al., 2021)). In Arabidopsis, apoplastic ROS is mainly produced by a family of NADPH oxidases located in the plasma membrane known as RESPIRATORY BURST OXIDASE PROTEINs (RBOHs) (Torres & Dangl, 2005). The production of ROS is often found closely linked to an increase in the concentration of cytosolic Ca^{2+} ($[Ca^{2+}]_{cyt}$), where the interplay between these signaling molecules is observed in immunity across kingdoms (Kadota et al., 2015; Steinhorst & Kudla, 2013). Interestingly, ROS and $[Ca^{2+}]_{cyt}$ are known signaling molecules acting downstream of several peptide ligand-receptor pairs. This includes the endogenous PAMPs ELICITOR PEPTIDE(PEP)1, PEP2 and PEP3 which function as elicitors of systemic responses against pathogen attack and herbivory (Huffaker et al., 2006; Ma et al., 2012; Qi et al., 2010), as well as the pathogen derived peptide ligands flagellin22 (flg22) and elongation factor thermo unstable(Ef-Tu) which bind and activate defense related RKs in the PM of the plant cell (Felix et al., 1999; Gómez-Gómez et al., 1999; Ranf et al., 2011).

The interplay between ROS and $[Ca^{2+}]_{cyt}$ has been well studied in the flg22 induced signaling system. The flg22 peptide interacts with the extracellular domain of the FLAGELLIN SENSING2 (FLS2) receptor kinase, which rapidly leads to an increase in $[Ca^{2+}]_{cyt}$ (Ranf et al., 2011). In a resting state, the co-receptor BRASSINOSTEROID INSENSITIVE1-ASSOCIATED RECEPTOR KINASE1/SERK3) (BAK1) and the cytoplasmic kinase BOTRYTIS-INDUCED KINASE1 (BIK1) form a complex with FLS2. Upon binding of flg22 to the FLS2 receptor, BIK1 is released from the receptor complex and activates intracellular signaling molecules through phosphorylation, among other, the PM localized RBOHD (Kadota et al., 2014; Li et al., 2014). The flg22 induced apoplastic ROS produced binds to PM localized Ca^{2+} channels on neighboring cells, activating Ca^{2+} influx into the cytosol. The cytosolic Ca^{2+} may bind to CALCIUM DEPENDENT PROTEIN KINASE5 (CDPKs) regulating RBOHD activity through phosphorylation. The Ca^{2+} dependent phosphorylation of RBOH enhances ROS production, which in turn leads to a propagation of the ROS/Ca^{2+} signal through the plant tissue (Dubiella et al., 2013)

A rapid increase in $[Ca^{2+}]_{cyt}$ is not only observed in peptide-ligand induced signaling. Similar $[Ca^{2+}]_{cyt}$ changes are observed as responses to developmental signals, such as extracellular auxin and environmental signals such as high salt conditions and drought(reviewed in (Kudla et al., 2018)). Also, $[Ca^{2+}]_{cyt}$ signals are observed in single cells during pollen tube and root hair growth (Monshausen et al., 2008; Sanders et al., 1999). How cells decipher the $[Ca^{2+}]_{cyt}$ changes into a specific cellular response is still largely unknown, however the cell contains a large toolkit of Ca^{2+} sensor proteins that may affect cellular function through changes in protein phosphorylation and gene expression. Each Ca^{2+} binding protein has specific affinities for Ca^{2+} allowing them to respond to different Ca^{2+} concentrations providing a specific cellular response (Geiger et al., 2010; Scherzer et al., 2012).

Given our previous studies showing IDA induced apoplastic ROS production (Butenko et al., 2014), and the known link between ROS and $[Ca^{2+}]_{cyt}$ response observed for other ligands such as flg22 (Dubiella et al., 2013), we sought to investigate if IDA induces a release of $[Ca^{2+}]_{cyt}$. Here we report that IDA is able to induce an intracellular release of Ca^{2+} in Arabidopsis root tips as well as in the AZ. Pursuing the tight connection between ROS and Ca^{2+} in other defense signaling systems we explored if the the observed production of ROS and Ca^{2+} in the IDA-HAE/HSL2 signaling pathway could be linked to the involvement of IDA in regulating plant defense (Patharkar et al., 2017). We show that a range of biotic and abiotic signals can induce *IDA* expression and we demonstrate that the IDA signal modulates responses of plant immune signaling. We propose that, in addition to regulating cell separation, IDA plays a role in enhancing a defense response in tissues undergoing cell separation thus providing the essential need for enhanced defense responses in tissue during the cell separation event.

Results:

IDA induces apoplastic production of ROS and elevation in cytosolic calcium-ion concentration

We have previously shown that a 12 amino acids functional IDA peptide, hereby referred to as mIDA (Sup Table 1), elicits the production of a ROS burst in *N.benthamiana* leaves transiently expressing *HAE* or *HSL2* (Butenko et al., 2014). To investigate whether mIDA could elicit a ROS burst in Arabidopsis, a luminol-dependent ROS assay on *hae hsl2* mutant rosette leaves expressing the full length HAE receptor under a constitutive promoter (*35S:HAE-YFP*) was performed. *hae hsl2 35S:HAE-YFP* leaf discs treated with mIDA emitted extracellular ROS, whereas no response was observed in wild-type (WT) leaves (Sup Fig.1a-c). We investigated the activity of the *HAE* and *HSL2* promoter in 22 days old Arabidopsis rosette leaves by cloning the promoters fused to the nuclear localized YFP-derived fluorophore Venus protein

(*pHAE:Venus-H2B*, *pHSL2:Venus-H2B*) and could observe a decrease in promoter activity in the oldest rosette leaves giving a possible explanation to the lack of mIDA induced ROS in true leaves (Sup Fig. 1d,e). Since rapid production of ROS is often linked to an elevation in $[Ca^{2+}]_{cyt}$ (Steinhorst & Kudla, 2013), we aimed to investigate if mIDA could induce a $[Ca^{2+}]_{cyt}$ response. We imaged Ca^{2+} in 10 days-old roots expressing the cytosolic localized fluorescent Ca^{2+} sensor R-GECO1 (Keinath et al., 2015). As a positive control for $[Ca^{2+}]_{cyt}$ release we added 1 mM extracellular ATP (eATP), which leads to a $[Ca^{2+}]_{cyt}$ elevation in the root tip within a minute after application (Fig. 1a) (Breiden et al., 2021). Following application of 1 µM mIDA, we detected an increase in $[Ca^{2+}]_{cyt}$ (Fig. 1a and Movie 1). R-GECO1 fluorescence intensities normalized to background intensities (ΔF/F) were measured from a region of interest (ROI) covering the meristematic and elongation zone of the root and revealed that the response starts 4-5 minutes after application of the mIDA peptide and lasts for 7-8 minutes (Fig. 1a). The signal initiated in the root meristematic zone from where it spread toward the elongation zone and root tip, a second wave was observed in the meristematic zone continuing with Ca^{2+} spikes. The signal amplitude was at a maximum within the elongation zone and decreased as the signal spread (Fig. 1a).

The $[Ca^{2+}]_{cyt}$ response in roots to the bacterial elicitor flg22 has previously been studied using the R-GECO1 sensor (Keinath et al., 2015). To better understand the specificity of the mIDA induced Ca^{2+} response, we aimed to compare the Ca^{2+} dynamics in mIDA treated roots to those treated with flg22. We observed striking differences in the onset and distribution of the Ca^{2+} signals. Analysis of roots treated with 1 µM flg22 showed that the Ca^{2+} signal initiated in the root elongation zone from where it spread toward the meristematic zone as a single wave and that the signal amplitude was at a maximum within the elongation zone and decreased as the signal spread (Fig. 1b, Movie 2). These observations indicate differences in tissue specificity of Ca^{2+} responses between mIDA and flg22, which we hypothesize depend on the cellular distribution of their cognate receptors. Indeed, when investigating the promoter activity of the *HAE*, *HSL2* and *FLS2* receptors by the use of nuclear localized transcriptional reporter lines we observed a different pattern of fluorescent nuclei in the roots (Fig. 1c,d,e). *pHAE:Venus-H2B* lines had fluorescent expression in the epidermis and stele of the elongation zone (Fig. 1c) and *pHSL2:Venus-H2B* lines in the lateral root cap, root tip and root meristem (Fig. 1d); while fluorescent nuclei were observed in the stele of the elongation zone in *pFLS2:Venus-H2B lines* (Fig. 1e). The different patterns of fluorescent nuclei observed for the three different receptor constructs could indeed explain the differences in the Ca^{2+} signatures triggered by mIDA and flg22. However, the receptors promoter activity show a broader expression pattern compared to the respective ligand induced $[Ca^{2+}]_{cyt}$ responses, indicating additional regulating factors for the observed $[Ca^{2+}]_{cyt}$ response.

To further investigate the mIDA induced Ca^{2+} response, we used a cytosolic localized Aequorin-based luminescence Ca^{2+} sensor (Aeq) (Knight et al., 1991). The Aeq sensor was chosen due to the well-

established use of this sensor in studies investigating peptide induced Ca^{2+} responses (Ranf et al., 2011) Removing the last Asparagine of the mIDA peptide (IDAΔN69; Sup Table 1) renders it inactive (Butenko et al., 2014). 7 days old *Aeq*-Seedlings treated with 1 µM IDAΔN69 did not show any increase in $[Ca^{2+}]_{cyt}$ (Sup Fig. 4a). To investigate if the $[Ca^{2+}]_{cyt}$ increase triggered by mIDA was dependent on extracellular Ca^{2+}, we pre-treated seedling with $LaCl_3$ and Ethylene glycol-bis (2-aminoethylether)- N, N, N′,N′-tetraacetic acid (EGTA). $LaCl_3$ and EGTA are inhibitors that block plasma membrane localized cation channels and chelate Ca^{2+} in the extracellular space, respectively (Knight et al., 1997). The mIDA induced response was abolished in *Aeq*-seedlings pre-incubated in 2 mM EGTA or 1 mM $LaCL_3$ (Sup Fig. 4b), indicating that the mIDA dependent $[Ca^{2+}]_{cyt}$ response depends on Ca^{2+} from the extracellular space.

Next we set out to investigate whether mIDA would trigger an increase in $[Ca^{2+}]_{cyt}$ in floral AZ cells. We utilized the Aeq expressing line and monitored $[Ca^{2+}]_{cyt}$ changes in flowers at different developmental stages (see Sup Fig. 5a for developmental stages [floral positions]) to 1 µM mIDA. Interestingly, only flowers at a the stage where there is an initial weakening of the AZ cell walls showed an increase in $[Ca^{2+}]_{cyt}$ (Sup Fig. 5). Flowers treated with mIDA prior to cell wall loosening showed no increase in luminescence (Sup Fig. 5), indicating that the mIDA triggered Ca^{2+} release in flowers correlates with the onset of the abscission process and the increase in *HAE* and *HSL2* expression at the AZ (Cai & Lashbrook, 2008; Patharkar & Walker, 2015). Using plants expressing the R-GECO1 sensor we performed a detailed investigation of the mIDA induced $[Ca^{2+}]_{cyt}$ response in flowers at position 6 which is the position where initial cell wall loosening occurs. The AZ region was analyzed for signal intensity values and revealed that the Ca^{2+} signal was composed of one wave (Fig. 2, Movie 3). The signal initiated close to the nectaries and spread throughout the AZ and further into the floral receptacle. Flowers treated with 1 µM IDAΔN69 did not show any increase in $[Ca^{2+}]_{cyt}$ in the AZ or receptacle, while a clear Ca^{2+} wave could be detected in the whole AZ, receptacle and proximal pedicel after treatment with eATP (Sup Fig.7, Sup Movie 2). Detailed investigation of *HAE* and *HSL2* promoter activity in flowers at position 6 shows restricted promoter activity to the AZ cells (Fig. 2b). The observed promoter activity correlates with the observed mIDA induced $[Ca^{2+}]_{cyt}$ response

The ROS producing enzymes, RBOHD and RBOHF, are not involved in the developmental process of abscission.

ROS and Ca^{2+} are secondary messengers that can play a role in developmental processes involving cell wall remodeling, but are also important players in plant immunity (Kärkönen & Kuchitsu, 2015). We therefore set out to investigate if the IDA induced production of ROS and increase in $[Ca^{2+}]_{cyt}$ function in the developmental process of abscission or if these signaling molecules form part of IDA modulated plant immunity.

The IDA induced Ca^{2+} response depends on Ca^{2+} from extracellular space (Sup Fig. 4b). Ca^{2+} transport over the plasma membrane is enabled by a variety of Ca^{2+} permeable channels, including the CYCLIC NUCLEOTIDE GATED CHANNELs (CNGCs). Various CNGCs are known to be involved in peptide ligand signaling in plants, including the involvement of CNGC6 and CNGC9 in CLAVATA3/EMBRYO SURROUNDING REGION40 signaling in roots (Breiden et al., 2021), and CNGC17 In phytosulfokine signaling (Ladwig et al., 2015). Using publicly available expression data we identified multiple CNGCs expressed in the AZ of Arabidopsis (Cai & Lashbrook, 2008) (Sup Fig. 8a, Sup Table. 3) and investigated if plants carrying mutations in the *CNGSs* genes expressed in AZs showed a defect in floral organ abscission. We observed no deficiency in floral abscission in the *cngc* mutants (Sup Fig. 8b), in contrast to what is observed in the *hae hsl2* mutant where all floral organs are retained throughout the inflorescence. Ca^{2+} partially activates members of the NOX family of nicotinamide adenine dinucleotide phosphate (NADPH) oxidases (RBOHs), key producers of ROS (Kadota et al., 2015). Two members of this family, *RBOHD* and *RBOHF* have high transcriptional levels in the floral AZs (Cai & Lashbrook, 2008) (Sup Fig. 8a, Sup Table. 3) and have been reported to be important in the cell separation event during floral abscission in Arabidopsis (Lee et al., 2018). We therefore set out to investigate if ROS production in AZ cells was dependent on RBOHD and RBOHF and to quantify to which degree these NADPH oxidases were necessary for organ separation. We treated AZs with the ROS indicator, H2DCF-DA, which upon contact with ROS has fluorescent properties, and observed ROS in both WT and to a lower extent in *rbohd rbohdf* flowers. In addition, we observed normal floral abscission in the *rbohd rbohf* double mutant flowers, indicating that the developmental progression of cell separation is not dependent on RBOHD and RBOHF (Sup Fig. 8c,d). These results are in stark contrast to what has previously been reported, where cell separation during floral abscission was shown to be dependent on RBOHD and RBOHF (Lee et al., 2018). We used a stress transducer to quantify the force needed to remove petals, the petal breakstrength (pBS) (Stenvik et al., 2008), from the receptacle of gradually older flowers along the inflorescence of WT and *rbohd rbohf* flowers. Measurements showed a significant lower pBS value for the *rbohd rbohf* mutant compared to WT at the developmental stage where cell loosening normally occurs, indicating premature cell wall loosening (Sup Fig. 8e). Furthermore, *rbohd rbohf* petals abscised one position earlier than WT (Sup Fig. 8e). Similar to Crick et al 2022,, we found no RBOHD and RBOHF dependent delay or absence of cell separation during floral abscission (Crick et al., 2022). Due to a known function of IDA in inducing ROS production (Sup Fig. 1), these results points towards a role for IDA in modulating additional responses to the process of cell separation.

IDA is upregulated by biotic and abiotic factors

In Arabidopsis, infection with the pathogen *P.syringae* induces cauline leaf abscission. Interestingly, stress induced cauline leaf abscission was reduced in plants with mutations in components of the IDA-HAE/HSL2 signaling pathway (Patharkar et al., 2017; Patharkar & Walker, 2016). In addition, upregulation of defense genes in floral AZ cells during the abscission process is altered in the *hae hsl2* mutant (Cai & Lashbrook, 2008; Niederhuth et al., 2013), indicating that the IDA-HAE/HSL2 signaling system may be involved in regulating defense responses in cells undergoing cell separation. We further investigated if *IDA* is upregulated by biotic and abiotic elicitors. Transgenic plants containing the *ß-glucuronidase (GUS*) gene under the control of the *IDA* promoter (*pIDA:GUS*) have previously been reported to exhibit *GUS* expression in cells overlaying newly formed LR primordia (Butenko et al., 2003; Kumpf et al., 2013). To investigate the expression of the *IDA* gene in response to biotic stress, *pIDA:GUS* seedlings were exposed to the bacterial elicitor flg22 and fungal chitin. Compared to the control seedlings, the seedlings exposed to flg22 and chitin showed a significant increase in *GUS* expression in LR primordia (Fig. 3a). Also, when comparing untreated root tips to those exposed to flg22 and chitin we observed a GUS signal in the primary root of flg22 and chitin treated roots (Fig. 3b). We used the fluorogenic substrate 4-methylumbelliferyl β-D-glucuronide (4-MUG) which is hydrolysed to the fluorochrome 4-methyl umbelliferone (4-MU) to quantify GUS-activity (Blazquez, 2007). A significant increase in fluorescence was observed for flg22 and chitin treated samples compared to untreated controls, (Fig. 3b), which was not observed when exposing seedlings to IDAΔN69 indicating that increased *IDA* expression is not triggered simply by the application of a peptide (Fig. 3). Spatial *pIDA:GUS* expression was also monitored upon abiotic stress. When *pIDA:GUS* seedling were treated with the osmotic agent mannitol or exposed to salt stress by NaCl, both treatments simulating dry soil, a similar increment in GUS signal was observed surrounding the LR primordia (Fig. 3). However, no *pIDA:GUS* expression was detected in the primary root (Fig. 3b). Taken together these results indicate an upregulation of *IDA* in tissue involved in cell separation processes such as the LR primordia and, interestingly, the root cap upon biotic stress. The process of cell separation is a fast and time-restricted response where cells previously protected by outer cell layers are rapidly exposed to the environment. These cells need strong and rapid protection against the environment, and we therefore aimed to investigate if IDA is involved in modulating immune responses in addition to inducing ROS and $[Ca^{2+}]_{cyt}$ responses.

mIDA can induce production of callose as a long term defense response

We aimed to investigate a possible role of IDA in regulating long-term defense responses in the plant, such as the production of callose. Callose deposition is a resulting hallmark of the late plant immunity responses that together with other events such as stomatal closure and production of ethylene leads to inhibition of pathogen multiplication and containment of disease (reviewed in (Wang et al., 2021)). Callose deposition is highly increased in response to flg22 (Gómez-Gómez et al., 1999). Promoter activity studies of *pHAE* and *pHSL2* indicates a weak activity of the promoters in the cotelydons, (Sup Fig. 1d) and we thus treated WT seedlings with 1 µM mIDA and measured the callose depositions per area in the cotyledons. We detected no difference to water treated controls indicating that either callose deposition is not a cellular outcome for mIDA treatment (Fig. 4a,b), or that receptor availability in the cotyledons is too low to observe a response We further tested if mIDA could induce callose depositions in cotyledons expressing the full length HAE receptor under a constitutive promoter (*35S:HAE-YFP*). An increase in the callose depositions per area upon mIDA treatment compared to water treated controls was observed in these lines (Fig. 4a,b). As a control, flg22 treated WT seedlings showed increased callose deposition, which was not observed in flg22 treated *fls2* seedlings (Fig. 4a,b). These results indicate that mIDA, is capable of promoting a HAE dependent deposition of callose as a long-term defense response.

mIDA triggers expression of defense-associated marker genes associated with innate immunity.

A -well-known part of a plants immune response is the enhanced transcription of genes involved in immunity. Transcriptional reprogramming mostly mediated by WRKY transcription factors takes place during microbe-associated molecular pattern (MAMP)- triggered immunity and is essential to mount an appropriate host defense response (Birkenbihl et al., 2017). We selected well-established defense-associated marker genes: *FLG22-INDUCED RECEPTOR-LIKE KINASE1* (*FRK1*), a specific and early immune-responsive gene activated by multiple MAMPs (Asai et al., 2002; He et al., 2006), *MYB51*, a WRKY target gene, previously shown to increase in response to the MAMP flg22 (Frerigmann et al., 2016) resulting in biosynthesis of the secondary metabolite indolic glucosinolates; and an endogenous danger peptide, ELICITOR PEPTIDE 3 (PEP3) (Huffaker et al., 2006). Seven days-old WT seedlings treated with 1 µM mIDA were monitored for changes in transcription of the aforementioned genes by RT-qPCR compared to untreated controls at two time points, 1 h and 12 h after treatment. All genes showed a significant transcriptional elevation 1 h after mIDA treatment (Fig. 5a). This in accordance with previous reports, where the expression of *FRK1* and *PEP3* was monitored in response to bacterial elicitors (He et al., 2006; Huffaker et al., 2006). After 12 h, *FRK1* and *PEP3* transcription in mIDA treated tissue was not

299 significantly different from untreated tissue; while transcription of *MYB51* in mIDA treated tissue
300 remained elevated after 12 h but was significantly lower compared to 1 h after mIDA treatment (Fig.
301 5a). Interestingly, the observed increase in transcription of the defense genes *MYB51* and *PEP3*, was
302 only partially reduced in the *hae hsl2* mutant (Sup Fig. 9). In contrast, *FRK1* showed higher
303 transcriptional levels in the *hae hsl2* mutant compared to WT (Sup Fig. 9). These results indicate that
304 also other receptors than HAE and HSL2 are involved in the mIDA-induced enhancement of the defense
305 genes *FRK1*, *MYB51* and *PEP3*.

306 We then analyzed a plant line expressing nuclear localized YFP from the MYB51 promoter
307 (*pMYB51:YFP*^{N}) (Poncini et al., 2017) treated with mIDA. Enhanced expression of p*MYB51:YFP* was
308 predominantly detected in the meristematic zone of the root after 7 h of mIDA treatment, compared to
309 a non-treated control (Fig. 5b). Moreover, comparison of mIDA induction with the elicitor-triggered
310 response of *pMYB51:YFP*^{N} to flg22 showed similar temporal expression in the root (Sup Fig. 10) .
311 Together, these data show that IDA can trigger a rapid increase in the expression of key genes involved
312 in immunity. We next investigated if the mIDA induced transcription of defense related genes was
313 similar to that induced by flg22. Seven days-old Col-0 WT seedlings were treated for 1h with mIDA, flg22
314 or a combination of mIDA and flg22 to explore potential additive effects. The relative increase in
315 transcription of the genes tested is similar when seedlings are treated with mIDA and flg22 (Fig. 6a).
316 However, when treating seedlings with both peptides the relative transcription of the genes of interest
317 increased substantially. To our surprise, the combined enhanced transcription when seedling where co-
318 treated with both flg22 and mIDA exceeds a simple additive effect of the two peptides. To investigate if
319 the observed increase is specific to a combination of mIDA and flg22, we investigated if co-treatment
320 with mIDA and PIP1, an endogenous DAMP peptide known to amplify the immune response triggered
321 by flg22, (Hou et al., 2014) gave a similar effect. Seedlings were treated for 1h with mIDA, PIP1 or a
322 combination of the peptides to explore additive effects. In contrast to what we observed with flg22, no
323 enhanced transcription of *FRK1*, *MYB51* and *PEP3* were observed after co-treatment with PIP1 and mIDA
324 (Sup Fig. 11). These results suggest a role of IDA in enhancing the defense response triggered by flg22.
325 To explore whether cells capable of undergoing cell separation in response to IDA and IDL peptides
326 could be expressing *HAE* or *HSL2* in combination with *FLS2* we made transcriptional reporter lines
327 expressing each of the receptors in fusion with either the nuclear localized YFP-derived fluorophore
328 Venus protein or the RFP-derived Tomato protein (*pRECEPTOR:Venus/Tomato-H2B*) and crossed the
329 lines to each other. Plants expressing both constructs were inspected for fluorescent nuclei in 7 day-old
330 roots as well as in floral organs of floral position 7. Fluorescent nuclei with overlapping Venus and
331 Tomato expression were observed both in the vascular tissue of the root, in cells surrounding LRs as
332 well as in cells of the AZs of plants expressing *pFLS2-Venus-H2B* and *pHAE-Tomat-H2B* (Fig. 6b). Similar

observations were done in the AZ of lines expressing *pFLS2-Venus-H2B* and *pHSL2-Tomat-H2B lines*, however in these lines overlapping fluorescent nuclei in roots were mainly observed in the epidermal cells surrounding the LR and in the root tip, as well as in the root cap (Fig. 6c). Based on these results we propose a role for IDA in enhancing immune responses in tissue undergoing cell separation, possibly by enhancing cellular responses activated by immune receptors, such as FLS2.

Discussion:

Several plant species can abscise infected organs to limit colonization of pathogenic microorganisms thereby adding an additional layer of defense to the innate immune system (Kissoudis et al., 2016; Patharkar et al., 2017). Also, in a developmental context, there is an induction of defense associated genes in AZ cells during cell separation and prior to the formation of the suberized layer that functions as a barrier rendering protection to pathogen attacks (Cai & Lashbrook, 2008; Niederhuth et al., 2013; Roberts et al., 2000; I. Taylor & J. C. Walker, 2018). Interestingly, the induction of defense genes during floral organ abscission is altered in *hae hsl2* plants (Niederhuth et al., 2013). It is largely unknown how molecular components regulating cell separation and how the IDA-HAE/HSL2 signaling pathway, contributes to modulation of plant immune responses. Here we show that the mature IDA peptide, mIDA, is involved in activating known defense responses in Arabidopsis, including the production of ROS, the intracellular release of Ca^{2+}, the production of callose and the transcription of genes known to be involved in defense (Sup Fig. 1, Fig. 1, Fig. 2, Fig. 5). We suggest a role for IDA in ensuring optimal cellular responses in tissue undergoing cell separation, regulating both development and defense.

The intracellular event occurring downstream of IDA is still partially unknown. Here we report the release of cytosolic Ca^{2+} as a new signaling component. Roots and AZs expressing the Ca^{2+} sensor R-GECO1, showed a $[Ca^{2+}]_{cyt}$ in response to mIDA. Moreover, the increased $[Ca^{2+}]_{cyt}$ in response to mIDA in flowers occurred only at stages where cell separation was taking place, linking the observed $[Ca^{2+}]_{cyt}$ response to the temporal point of abscission and the need for an induced local defense response. During floral development the expression of the *HAE* and *HSL2* receptors increase prior to the onset of abscission (Cai & Lashbrook, 2008) and may account for the temporal mIDA induced $[Ca^{2+}]_{cyt}$ response observed.

Based on these results, it is likely that the expression of the receptors is the limiting factor for a cells ability to respond to the mIDA peptide with a $[Ca^{2+}]_{cyt}$ response. However, promoter activity of the receptors are observed in a broader area of the root than the observed $[Ca^{2+}]_{cyt}$ response. As an example, *pHSL2* is found

to have a localized activation in the root tip, and when HSL2 is activated by IDL1 be involved in the regulation of cell separation during root cap sloughing (Shi et al., 2018). IDL1 and IDA have a high degree of similarity in the protein sequence, and *IDL1* expressed under the *IDA* promoter can fully rescue the abscission phenotype observed in the *ida* mutant (Stenvik et al., 2008). We can assume that IDL1 activates similar signaling components in the root cap as those used by IDA. Despite the expression of HSL2 and the involvement of the receptor in root cap sloughing, no $[Ca^{2+}]_{cyt}$ response is observed in this region when plants are treated with the IDA peptide. The absence of an observed $[Ca^{2+}]_{cyt}$ response in the root tip indicates that $[Ca^{2+}]_{cyt}$ is most likely not involved in the cell separation process during root cap sloughing, or that cells involved in this process only are able to induce a $[Ca^{2+}]_{cyt}$ response at a specific developmental time point. Thus, in addition to receptor availability, other factors must be involved in regulating the $[Ca^{2+}]_{cyt}$ response. It is intriguing that the mIDA cellular output is similar to that of flg22 (Kadota et al., 2015; Kadota et al., 2014) yet shows some distinct differences. The spatial distribution of the Ca^{2+} wave originated by mIDA differs from that of flg22. The *rbohd rbohf* mutant shows ROS production in the AZ, indicating that other NADPH oxidases or cell wall peroxidases expressed in the AZ may be involved in ROS production, in contrast to the importance of RBOHD RBOHF in flg22 signaling (Kadota et al., 2015). This suggests that while IDA and flg22 share many components for their signal transduction, such as the BAK1 co-receptor (Chinchilla et al., 2007; X. Meng et al., 2016) and MAPK cascade (Asai et al., 2002; Cho et al., 2008), there are other specific components that are likely important to provide differences in signaling. Despite the observation of the numerous defense related responses to mIDA, we cannot exclude that the mIDA induced $[Ca^{2+}]_{cyt}$ and rises in ROS levels may also have an intrinsic developmental role such as modulating cell wall properties and cell expansion similar to what is observed during FERONIA (FER) signaling (Dünser et al., 2019; Wei Feng et al., 2018). To further decipher the importance of the mIDA induced Ca^{2+} and ROS in defense it will be important to identify the specific signaling components responsible for this cellular output in addition to investigating the susceptibility of mutants to pathogen exposure.

Interestingly, FLS2 arrangement into nanoscale domains at the PM is dependent on FER. FLS2 becomes more disperse and mobile in *fer* mutants, implying a role for FER in regulating FLS2 activity (Gronnier et al., 2022). Also altering of the cell wall affects FLS2 nanoscale organization (McKenna et al., 2019). Formation of nanoscale domains containing the HAE and HSL2 receptors may be an important signaling step in the IDA-HAE/HSL2 signaling pathway. From our promoter analysis we clearly see overlapping activity of the *HAE* and *HSL2* promoters with the *FLS2* promoter *in planta*, providing the possibility that the receptors are localized at the PM of the same cells and can have coordinated signaling events. An intriguing thought is a possible co-localization of HAE and HSL2 with FLS2 in nanoscale domains, making a signaling unit possible to involve multiple different receptors responsible for the signaling outcome observed. In this paper, we show that co-treatment with mIDA and flg22 induces an enhanced

transcription of defense related genes. How FLS2, HAE and HSL2 communicate at the plasma membrane of the responsive cells may give the answers to the molecular mechanisms behind the augmented transcriptional regulation observed when co-treatment of mIDA and flg22 is performed (Fig. 6). We can investigate possible interaction partners of HAE and HSL2 looking at available data from a sensitized high-throughput interaction assay between extracellular domains (ECDs) of 200 Leucine Rich Repeat (LRR) (Smakowska-Luzan et al., 2018). Interestingly, LRR-RLKs known to play a function in biotic or abiotic stress responses, such as RECEPTOR-LIKE KINASE7 (RLK7), STRUBBELIG-RECEPTOR FAMILY3 , RECEPTOR-LIKE PROTEIN KINASE 1 and FRK1, are found to interact mainly with HSL2, whereas HAE shows interaction with LRRs mainly involved in development (Sup Fig. 12). RLK7 has recently been identified as an additional receptor for CEP4, involved in regulating cell surface immunity and response to nitrogen starvation, indication a role of RLK7 as an additional receptor regulating defense responses in known peptide-receptor complexes (Rzemieniewski et al., 2022). It would be interesting to investigate a possible role of RLK7 in IDA-HAE/HSL2 signaling as a signaling partner in the observed IDA-induced defense responses.

In this paper, we propose a model where the IDA-HAE/HSL2 signaling pathway modulates defense responses in tissues undergoing cell separation. It is beneficial for the plant to ensure an upregulation of defense responses in tissues undergoing cell separation as a precaution against pathogen attack. This tissue is a major entry route for pathogens, and by combining the need of both the IDA peptide and the pathogen molecular pattern, such as flg22, for the induction of a strong defense response, the plant ensures maximum immunity in the most prone cells without spending energy inducing this in all cells (Fig. 7). Such a molecular mechanism, where the presence of mIDA in tissue exposed to stress leads to maximum activation of the immune responses, will ensure maximal protection of infected cells during cell separation, cells which are major potential entry routes for invading pathogens.

Movies

Movie 1: $[Ca^{2+}]_{cyt}$ dynamics in R-GECO1 expressing root tip in response to 1 µM mIDA. 10 days-old roots were treated with 1 µM mIDA and changes in $[Ca^{2+}]_{cyt}$ was recorded over time. Response shown as normalized fluorescence intensities (ΔF/F). Images were recorded with a frame rate of 5 seconds. Movie corresponds to measurements shown in Fig. 1a. Representative response from 10 roots. Time shown as, hh:mm:ss.

Movie 2: $[Ca^{2+}]_{cyt}$ dynamics in R-GECO1 expressing root tip in response to 1 µM flg22 10 days-old roots were treated with 1 µM flg22 and changes in $[Ca^{2+}]_{cyt}$ was recorded over time. Response shown as normalized fluorescence intensities (ΔF/F). Images were recorded with a frame rate of 5 seconds. Movie corresponds to measurements shown in Fig. 1b. Representative response from 7 roots. Time shown as, hh:mm:ss.

Movie 3: $[Ca^{2+}]_{cyt}$ dynamics in R-GECO1 expressing AZ in response to 1 µM mIDA. Flowers at position 6 were treated with 1 µM mIDA and changes in $[Ca^{2+}]_{cyt}$ was recorded over time. Response shown as normalized fluorescence intensities (ΔF/F). Images were recorded with a frame rate of 5 seconds. Movie corresponds to measurements shown in Fig. 2a. Representative response from 8 flowers. Time shown as, hh:mm:ss.

Sup Movie 1: $[Ca^{2+}]_{cyt}$ dynamics in R-GECO1 expressing root tip in response to 1 mM eATP. 1 mM eATP will induce a strong increase in $[Ca^{2+}]_{cyt}$ and was added as a last treatment to all roots acting as a positive control. Response shown as normalized fluorescence intensities (ΔF/F). Images were recorded with a frame rate of 5 seconds. Movie corresponds to measurements shown in Fig. 1a. Representative response from 10 roots. Time shown as, hh:mm:ss.

Sup Movie 2: $[Ca^{2+}]_{cyt}$ dynamics in R-GECO1 expressing AZ in response to to 1 µM of the inactive IDA peptide, $IDA^{\Delta N69}$. Flowers at position 6 were treated with 1 µM $IDA^{\Delta N69}$ and changes in $[Ca^{2+}]_{cyt}$ was recorded over time. Response shown as normalized fluorescence intensities (ΔF/F). Images were recorded with a frame rate of 5 seconds. Movie corresponds to measurements shown in Sup Fig. 6. Representative response from 7 flowers. Time shown as, hh:mm:ss.

Methods

Accession numbers of genes studied in this work:

HSL2 At5g65710, IDA At1g68765, FLS2 At5g46330, HAE At4g28490, MYB51 At1g18570, RBOHD At5g47910, RBOHF At1g64060, PEP3 At5g64905, WRKY33 At2g38470, FRK1 At2g19190. Plant lines used in this work: Ecotype Colombia-0 (Col-0) was used as wild type (WT). Mutant line: *hae* (SALK_021905), *hsl2*, (SALK_030520), *fls2* (SALK_062054), *rbohd* (SALK_070610), *rbohf* (SALK_059888), *cngc1* (SAIL_443), *cngc2* (SALK_066908), *cngc4* (SALK_081369), *cngc5* (SALK_149893), *cngc6* (SALK_064702), *cngc9* (SAIL_736), *cngc12* (SALK_093622). SALK lines were provided from Nottingham Arabidopsis Stock Centre (NASC).

Plant lines

The pIDA:GUS, pHSL2:Venus-H2B and pMYB51:YFPN lines have been described previously (Kumpf et al., 2013; Poncini et al., 2017; Shi et al., 2018).The promoters of HAE (1601 bp (Kumpf et al., 2013) and HSL2

(2300 bp (Sto et al., 2015))were available in the pDONRZeo vector (Thermo Fischer Scientific). Sequences corresponding to the FLS2 promoter (988 bp (Robatzek et al., 2006)) were amplified from WT DNA (primers are listed in table 2) and cloned into the pDONRZeo vector (Thermo Fischer Scientific). All promoter constructs were further recombined into the promotor:Venus (YFP)-H2B and Tomato-H2B destination vectors (Somssich et al., 2016) using the Invitrogen Gateway cloning system (Thermo Fischer Scientific). Constructs were transformed into *Agrobacterium tumefaciens* (A.tumefaciens) C58 and the floral dip method (Clough & Bent, 1998) was used to generate transgenic lines. Single-copy homozygous plant lines were selected and used in this study. The CDS of HAE was cloned into the pEarleyGate101 destination vector (Earley et al., 2006) using the Invitrogen Gateway cloning system and transformed into A.tumefaciens C58 and further used to generate the *35S:HAE:YFP* lines.

Growth conditions

Plants were grown in long day conditions (8 h dark and 16 h light) at 22 °C. Seeds were surface sterilized and plated out on MS-2 plates, stratified for 24 h at 4 °C and grown on plates for 7 days before transferred to soil.

Peptide sequences

Peptides used in this study were ordered from BIOMATIK. Peptide sequences are listed in Supplementary Table 1.

Primers

Primers for genotyping and generation of constructs were generated using VectorNTI. Gene specific primers for RT-qPCR were generated using Roche Probe Library Primer Design. All primers are listed in Supplementary Table 2.

Histochemical GUS assay

Seven days-old seedlings were pre-incubated for 12 h in liquid MS-2 medium containing stimuli of interest; 1 µM peptide (table 1), 60 mM Mannitol (M4125 – Sigma), 20 µg/mL Chitin (C9752 – Sigma), 50 mM NaCl and then stained for GUS activity following the protocol previously described (Stenvik et al., 2008). Roots were pictured using a Zeiss Axioplan2 microscope with an AxioCam HRc, 20x air objective. The assay was performed on 10 individual roots and the experiment was repeated 3 times.

Fluorescent GUS assay

Seven days-old seedlings were pre-incubated for 12 h in liquid MS-2 medium with or without stimuli of interest; 1 µM peptide (table 1), 60 mM Mannitol (M4125 – Sigma), 20 µg/mL Chitin (C9752 – Sigma),

50 mM NaCl. After treatment, 10 seedlings were incubated in wells containing 1 mL reaction mix described in (Blazquez, 2007) containing: 10 mM EDTA (pH 8.0), 0,1 % SDS, 50 mM Sodium Phosphate (pH 7.0), 0,1 % Triton X-100, 1 mM 4-MUG (, M9130-Sigma) and incubated at 37 °C for 6 h. Six 100 µl aliquots from each well were transferred to individual wells in a microtiter plate and the reaction was stopped by adding 50 µl of stop reagent (1 M Sodium Carbonate) to each well. Fluorescence was detected by the use of a Wallac 1420 VICTOR2 microplate luminometer (PerkinElmer) using an excitation wavelength of 365 nm and a filter wavelength of 430 nm. Each experiment was repeated 3 times.

Confocal laser microscopy of roots and flowers expressing promoter:Venus/YFP-H2B and promoter: Tomato-H2B construct

Imaging of 7 days-old roots was performed on a LSM 880 Airyscan confocal microscope equipped with two flanking PMTs and a central 32 array GaAsP detector. Images were acquired with Zeiss Plan-Apochromat 20x/0.8 WD=0.55 M27 objective and excited with laser light of 405 nm, 488 nm and 561 nm. Roots were stained by 1 µM propidium iodide for 10 min and washed in dH_2O before imaging. Imaging of flowers was performed on an Andor Dragonfly spinning disk confocal using an EMCCD iXon Ultra detector. Images were acquired with a 10x plan Apo NA 0,45 dry objective and excited with laser light of 405 nm, 488 nm and 561 nm. Maximum intensity projections of z-stacks were acquired with step size of 1,47 µm. Image processing was performed in FIJI 51. These steps are: background subtraction, gaussian blur/smooth, brightness/contrast. Imaging was performed at the NorMIC Imaging platform.

Calcium imaging using the R-GECO1 sensor

$[Ca^{2+}]_{cyt}$ in roots were detected using WT plants expressing the cytosolic localized single-fluorophore based Ca^{2+} sensor, R-GECO1 in Col-0 background (Keinath et al., 2015). Measurements were performed using a confocal laser scanning microscopy Leica TCS SP8 STED 3X using a 20x multi NA 0.75 objective. Images were recorded with a frame rate of 5 seconds at 400 Hz. Seedling mounting was performed as described in (Krebs & Schumacher, 2013). The plant tissues were incubated overnight in half strength MS, 21°C and continuous light conditions before the day of imaging. $[Ca^{2+}]_{cyt}$ in the abscission zone were detected using WT plants expressing R-GECO1 (Keinath et al., 2015). Abscission zones of position 7 were used. Mounting of the abscission zones were performed using the same device as for seedlings (Krebs & Schumacher, 2013). The abscission zones were incubated in half strength MS medium for 1 h before imaging. Measurements were performed with a Zeiss LSM880 Airyscan using a Plan-Apochromat 10×

air NA 0.30 objective. Images were recorded with a frame rate of 10 seconds. R-GECO1 was excited with a white light laser at 561 nm and its emission was detected at 590 nm to 670 nm using a HyD detector. Laser power and gain settings were chosen for each experiment to maintain comparable intensity values. For mIDA and flg22 two-fold concentrations were prepared in half strength MS. mIDA or flg22 were added in a 1:1 volume ratio to the imaging chamber (final concentration 1 µM). ATP was prepared in a 100-fold concentration in half strength MS and added as a last treatment in a 1:100 volume ratio (final concentration 1 mM) to the imaging chamber as a positive control for activity of the R-GECO1 sensor (Movie 3). Image processing was performed in FIJI. These steps are: background subtraction, gaussian blur, MultiStackReg v1.45 (http://bradbusse.net/sciencedownloads.html), 32-bit conversion, threshold. Royal was used as a look up table. Fluorescence intensities of indicated ROIs were obtained from the 32-bit images (Krebs & Schumacher, 2013). Normalization was done using the following formula $\Delta F/F = (F-F0)/F0$ where F0 represents the mean of at least 1 min measurement without any treatment. R-GECO1 measurements were performed at the Center for Advanced imaging (CAi) at HHU and at NorMIC Imaging platform at the University of Oslo.

Calcium measurements using the Aequorin (pMAQ2) sensor

$[Ca^{2+}]_{cyt}$ in seedlings and flowers were detected using WT plants expressing p35S-apoaequorin (pMAQ2) located to cytosol (Aeq) (Knight et al., 1991; Ranf et al., 2011). Aequorin luminescence was measured as previously described (Ranf et al., 2012). Emitted light was detected by the use of a Wallac 1420 VICTOR2 microplate luminometer (PerkinElmer). Differences in Aeq expression levels due to seedling size and expression of sensor were corrected by using luminescence at specific time point (L)/Max Luminescence (Lmax). Lmax was measured after peptide treatment by individually adding 100 µL 2 M $CaCl_2$ to each well and measuring luminescence constantly for 180 seconds (Ranf et al., 2012). 2 M $CaCl_2$ disrupts the cells and releases the Aeq sensor into the solution where it will react with Ca^{2+} and release the total possible response in the sample (Lmax) in form of a luminescent peak. A final concentration of 1 µM mIDA was added to each wells at the start of measurements. For inhibitor treatments, Aeq-seedlings were incubated in in 2 mM EGTA (Sigma-Aldrich) or 1 mM $LaCL_3$ (Sigma-Aldrich) O/N before measurements. For seedlings 3 independent experiments were performed with 12 replications in each experiment. For flowers 3 independent experiments were performed with 4-6 replications in each experiment.

Measurements of reactive oxygen species (ROS)

ROS production was monitored by the use of a luminol-dependent assay as previously described (Butenko et al., 2014) using a Wallac 1420 VICTOR2 microplate luminometer (PerkinElmer). Arabidopsis leaves expressing *35S:HAE:YFP* were cut into leaf discs and incubated in water overnight before

561 measurements. A final concentration of 1 µM mIDA was added to each well at the start of
562 measurements. All measurements were performed on 6 leaf discs and each experiment was repeated
563 3 times.

564 ROS stain (H2DCF-DA)

565 Flowers at position 6 were gently incubated in staining solution (25 µM (2',7'-dichlorodihydrofluorescein
566 diacetate) (H2DCF-DA) (Sigma-Aldrich, D6883), 50 mM KCL, 10 mM MES) for 10 min and further washed
567 3 times in wash solution (50 mM KCL, 10 mM MES). For the *hae hsl2* mutant the floral organs were
568 forcibly removed immediately before imaging. Imaging was done using a Dragonfly Airy scan spinning
569 disk confocal microscope, excited by a 488 nm laser. A total of 9 flowers per genotype were imaged.
570 The experiment was repeated 2 independent times.

571 Callose deposition staining and quantification

572 Callose deposition experiments were conducted as per (Luna et al., 2011) with modifications. Seeds
573 from WT and *fls2* were vapor-phase sterilized for 4 h. Seeds were transferred to 12-well plates
574 containing 1 mL of filter-sterilized MS medium and 0. 5 % MES with a final pH of 5.7, and stratified in
575 the dark at 4 °C for 2 days. Plates were consecutively transferred to a growth chamber with 16 h of light
576 (150µE m-2 s-1)/8h darkness cycle at 22°C. On the seventh day, growth medium was refreshed under
577 sterile conditions. On the eight day the treatments were applied: addition of 10 µL of water (mock); 10
578 µL of 100 µM flg22; or 10 µL of 100 µM mIDA (final peptide concentrations of 1 µM). After 24 h the
579 growth medium was replaced with 9 5% ethanol and incubated overnight. Ethanol was replaced with
580 an 8 M NaOH softening solution and incubated for 2 h. Seedlings were washed 3 times in water and
581 immediately transferred to the aniline blue staining solution (100 mM KPO4-KOH, pH 11; 0.01 % aniline
582 blue). After 2 h of staining, the seedlings were mounted on 50 % glycerol and imaged under a ZEISS
583 epifluorescence microscope with UV filter (BP 365/12 nm; FT 395 nm; LP 397 nm). Image analysis was
584 performed on FIJI (Schindelin et al., 2012). In brief, cotyledons were cropped and measured the leaf
585 area. Images were thresholded to remove autofluorescence and area of depositions measured to
586 calculate the ratio of callose deposition area per cotyledon area unit. Between 9-12 seedlings were
587 analyzed per genotype x treatment combination.

588 Real time quantitative PCR (RT-qPCR)

589 Seven days-old Arabidopsis seedlings (WT, *hae hsl2*) grown vertically on ½ sucrose MS-2 plates were
590 transferred to liquid ½ MS-2 medium (non-treated) and liquid ½ MS-2 medium containing 1 µM peptide
591 (Supplementary Table 1) and incubated in growth chambers for 1 h or 12 h. Seedlings were flash-frozen
592 in liquid nitrogen before total RNA was extracted using SpectrumTM Plant Total RNA Kit (SIGMA Aldrich).

cDNA synthesis was performed as previously described (Grini et al., 2009). RT-qPCR was performed according to protocols provided by the manufacturer using FastStart Essential DNA Green Master (Roche) and LightCycler96 (Roche) instrument. ACTIN2 was used to normalize mRNA levels as described in (Grini et al., 2009). Two-three biological replicates and 4 technical replicates including standard curves were performed for each sample.

Petal Break strength (pBS)

The force required to remove a petal at a given position on the inflorescence was measured in gram equivalents using a load transducer as previously described (Stenvik et al., 2008). Plants were grown until they had at least 15 positions on the inflorescence. A minimum of 15 petals per position were measured. pBS measurements were performed on WT, *rbohd rbohf* (SALK_070610 SALK_059888) and *hae hsl2* (SALK_021905 SALK_030520) plants.

Statistical methods

Two tailed students t-test ($p < 0.05$) was used to identify significant differences in the fluorescent GUS assay by comparing treated samples to untreated samples of the same plant line. Statistical analysis of the RT-qPCR results was performed on all replicas using ONE-WAY or TWO-WAY ANOVA (as stated in the figure text) and post-hoc Tukey's test ($p < 0.05$). Two tailed students t-test with ($p < 0.05$) was used in the petal break strength (pBS) measurements to identify significant differences from WT at a given position on the inflorescence.

Acknowledgements

We thank M.K. Anker, I.M. Stø, V. Iversen and R. Falleth for technical assistance in the laboratory and phytotrone. We thank the NorMic Imaging platform for the use and technical support. This work was supported by the Research Council of Norway (grant 230849) to V.O.Lalun and M.A.Butenko Work by R. Simon and and M.Breiden was supported through CEPLAS.

Author contributions

V.O.L generated Arabidopsis lines and constructs, tested IDA expression to biotic and abiotic stress, performed gene expression studies, callose deposition assays, phenotypic analysis of mutants and ROS measurements. V.O.L and M.B. performed Ca^{2+} measurements. V.O.L, S. G-T., M.B., R.S and M.A.B

622 designed experiments, analyzed data, and drafted the manuscript. V.O.L and M.A.B wrote the paper
623 with input from all authors.

624

625 Competing interests

626 The authors have no competing interests.

627 Materials and correspondence

628 Correspondence to Melinka A. Butenko, m.a.butenko@ibv.uio.no

629

630

631 Supplementary Tables

632 Sup Table. 1: Peptide sequences

Peptide	Amino acid sequence
mIDA	PIPPSA**o**SKRHN
flg22	QRLSTGSRINSAKDDAAGLQIA
IDA$^{\Delta N69}$	PIPPSA**o**SKRH
PIP1	RFVKHSG**o**SPSGPGH

633 (**o** = hydroxyproline)

634

635 Sup Table. 2: Primers sequences and function

Function	Primer name	Primer sequence 5'-3'
Cloning promoter FLS2	PromFLS2 -988bp Attb1	5'GGGGACAAGTTTGTACAAAAAAGCAGGCTTA GAAGTTGTGAATTGTGAT'3
Cloning promoter FLS2	PromFLS2 -988bp Attb2	5'GGGGACCACTTTGTACAAGAAAGCTGGGTA GGTTTAGACTTTAGAAGA'3

Genotype hsl2	Hsl2 LP	5'CGTCTTGAGCTAGCCAACAAC'3
Genotype hsl2	Hsl2 RP	5'GTCCAATCAAGTGGAGAAACG'3
Genotype hae	Haesa LP	5'CACCTTCCTTCTCTCCATTCC'3
Genotype hae	Haesa RP	5'GTTCGAGAAGTGACAAGCGAG'3
Genotype SALK-lines	Lbb1-	5'GCGTGGACCGCTTGCTGCAACT'3
Genotype rbohd SALK_070610C	LP_SALK_070610C	5'TTTCAACGCCTTTTGGTACAC'3
Genotype rbohd SALK_070610C	RP_SALK_070610C	5'GTTACCTATTCTTTTGCCGGG'3
Genotype rbohf SALK_059888	LP_SALK_059888	5'CAAAGAGCTCTTCGTGGTTTG'3
Genotype rbohf SALK_059888	RP_SALK_059888	5'TCTCTATTGTATCTTGTGTCACCG'3
Genotype fls2 SALK_062054	FLS2_SALK_062054 Fw	5'GGTTCGATTCCTTCTGGAATC'3
Genotype fls2 SALK_062054	FLS2_SALK_062054 Rv	5'CCTGAGTTTTTGAAGCTTCCC'3
qPCR	33.FRK1 Fw	5'AACTTAGGAGACTATTTGGCAGGTAA'3
qPCR	33.FRK1 Rv	5'TGCATCTAATGATATCTTCAACCTCT'3
qPCR	63.PEP3 Fw	5'GCGAGGAAGATGAGAGTATCG'3
qPCR	63.PEP3 Rv	5'TCAATGGTCATGCCATCTTCT'3
qPCR	91.MYB51 Fw	5'GGCCAATTATCTTAGACCTGACA'3
qPCR	91.MYB51 Rv	5'CCACGAGCTATAGCAGACCATT'3
qPCR reference gene	act2int2 sense	5'CCCTGAGGAGCACCCAGTTCTACTC'3
qPCR reference gene	act2int2 antisense	5'CCGCAAGATCAAGACGAAGGATAGC'3

636

637

638 **Sup Table. 3: Relative expression of genes of the CNGC and RBOH gene families during the onset of**
639 **abscission** (data from (Cai & Lashbrook, 2008)). See Sup Fig. 5a for flower developmental stages (p2-
640 p6). CNGC = CYCLIC NUCLEOTIDE GATED CHANNEL, RBOH = RESPIRATORY BURST OXIDASE PROTEIN,
641 IDA = INFLORESCENCE DEFICIENT IN ABSCISSION, HSL2 = HAESA-LIKE 2.

642

Locus ID	*Name/Flower developmental stages*	p2	p3	p4	p5	p6
CNGCs						
At5g53130	*CNGC1*	291,9217	310,4919	495,7432	478,204	469,1732
At5g15410	*CNGC2*	1052,741	707,3286	626,9068	564,8327	557,5938
At5g54250	*CNGC4*	123,1472	193,9821	166,5376	176,2532	152,5896
At5g57940	*CNGC5*	691,9364	691,89	689,136	693,1147	396,6692
At2g23980	*CNGC6*	378,221	537,386	463,2181	502,9967	418,4082
At1g15990	*CNGC7*	42,53905	4,013366	3,253884	4,808204	7,830878
At1g19780	*CNGC8*	127,1805	63,14431	12,499	26,13849	11,25919
At4g30560	*CNGC9*	1115,91	673,8271	209,3169	197,1013	218,3005
At1g01340	*CNGC10*	92,29875	237,8649	115,0834	167,9021	116,888
At2g46440; At2g46430	*CNGC11; CNGC3*	3,751632	19,02687	101,7517	75,33781	97,46469
At2g46450	*CNGC12*	73,57635	154,3836	194,2215	256,2537	199,3865
At4g01010	*CNGC13*	26,81946	27,13074	36,37046	13,7691	35,73786
At2g24610	*CNGC14*	24,62137	24,55057	37,37278	32,75482	26,07159
At2g28260	*CNGC15*	26,53137	39,16623	21,37623	29,06457	22,87302
At3g48010	*CNGC16*	40,68595	12,40819	1,003874	1,432107	6,756874
At4g30360	*CNGC17*	127,9115	162,4681	216,6674	191,8812	157,5401
At5g14870	*CNGC18*	189,1577	98,09141	37,70282	29,79446	15,07226
At3g17690	*CNGC19*	4,532605	1,830825	5,04741	5,905303	3,699505
At3g17700	*CNGC20*	52,89588	94,00054	107,4842	78,12915	40,67315
RBOHs						
At5g07390	*RBOHA*	4,185314	3,00695	3,438994	3,472965	3,41175
At1g09090	*RBOHB*	1,006999	1,055189	1,824025	1,175719	1,696683
At5g51060	*RBOHC*	20,71598	69,57144	13,97975	9,319057	8,847032
At5g60010	*RBOHD*	1150,998	603,4534	601,9696	805,7448	885,5323
At1g19230	*RBOHE*	7,372654	6,069166	4,934652	9,946411	6,019031
At1g64060	*RBOHF*	200,0895	222,463	297,3	449,7607	873,9841
At4g25090	*RBOHG*	4,048472	3,046103	3,217067	2,755258	5,142675
At5g60010	*RBOHH*	94,40216	65,08288	18,12167	26,1705	18,26213
At4g11230	*RBOHI*	11,76717	10,91102	17,55314	17,93307	11,61079
At3g45810	*RBOHJ*	99,10577	95,51017	71,29349	66,03646	63,07515
IDA signaling pathway						
At1g68765	*IDA*	8,245425	6,850307	32,37852	224,6666	1268,797

At4g28490	*HAESA*	336,4576	811,4685	4950,168	6327,225	8082,581
At5g65710	*HSL2*	2517,483	4441,616	7633,162	8056,462	7993,356

643

644

References:

Agustí, J., Merelo, P., Cercós, M., Tadeo, F. R., & Talón, M. (2009). Comparative transcriptional survey between laser-microdissected cells from laminar abscission zone and petiolar cortical tissue during ethylene-promoted abscission in citrus leaves. *BMC Plant Biology*, *9*(1), 127. https://doi.org/10.1186/1471-2229-9-127

Asai, T., Tena, G., Plotnikova, J., Willmann, M. R., Chiu, W. L., Gomez-Gomez, L., Boller, T., Ausubel, F. M., & Sheen, J. (2002). MAP kinase signalling cascade in Arabidopsis innate immunity. *Nature*, *415*(6875), 977-983. https://doi.org/10.1038/415977a

Birkenbihl, R. P., Kracher, B., & Somssich, I. E. (2017). Induced Genome-Wide Binding of Three Arabidopsis WRKY Transcription Factors during Early MAMP-Triggered Immunity. *Plant Cell*, *29*(1), 20-38. https://doi.org/10.1105/tpc.16.00681

Blazquez, M. (2007). Quantitative GUS Activity Assay in Intact Plant Tissue. *CSH Protoc*, *2007*, pdb.prot4688. https://doi.org/10.1101/pdb.prot4688

Bleecker, A. B., & Patterson, S. E. (1997). Last exit: senescence, abscission, and meristem arrest in Arabidopsis. *Plant Cell*, *9*(7), 1169-1179. https://doi.org/10.1105/tpc.9.7.1169

Breiden, M., Olsson, V., Blümke, P., Schlegel, J., Gustavo-Pinto, K., Dietrich, P., Butenko, M. A., & Simon, R. (2021). The Cell Fate Controlling CLE40 Peptide Requires CNGCs to Trigger Highly Localized Ca2+ Transients in Arabidopsis thaliana Root Meristems. *Plant Cell Physiol*, *62*(8), 1290-1301. https://doi.org/10.1093/pcp/pcab079

Butenko, M. A., Patterson, S. E., Grini, P. E., Stenvik, G.-E., Amundsen, S. S., Mandal, A., & Aalen, R. B. (2003). *INFLORESCENCE DEFICIENT IN ABSCISSION* Controls Floral Organ Abscission in Arabidopsis and Identifies a Novel Family of Putative Ligands in Plants. *Plant Cell*, *15*, 2296-2307.

Butenko, M. A., Wildhagen, M., Albert, M., Jehle, A., Kalbacher, H., Aalen, R. B., & Felix, G. (2014). Tools and Strategies to Match Peptide-Ligand Receptor Pairs. *Plant Cell*, *26*(5), 1838-1847. https://doi.org/10.1105/tpc.113.120071

Cai, S., & Lashbrook, C. C. (2008). Stamen abscission zone transcriptome profiling reveals new candidates for abscission control: enhanced retention of floral organs in transgenic plants overexpressing Arabidopsis ZINC FINGER PROTEIN2. *Plant Physiol*, *146*(3), 1305-1321. https://doi.org/10.1104/pp.107.110908

Castro, B., Citterico, M., Kimura, S., Stevens, D. M., Wrzaczek, M., & Coaker, G. (2021). Stress-induced reactive oxygen species compartmentalization, perception and signalling. *Nat Plants*, *7*(4), 403-412. https://doi.org/10.1038/s41477-021-00887-0

Chinchilla, D., Zipfel, C., Robatzek, S., Kemmerling, B., Nurnberger, T., Jones, J. D., Felix, G., & Boller, T. (2007). A flagellin-induced complex of the receptor FLS2 and BAK1 initiates plant defence. *Nature*, *448*(7152), 497-500. https://doi.org/10.1038/nature05999

Cho, S. K., Larue, C. T., Chevalier, D., Wang, H., Jinn, T. L., & Zhang, S. (2008). Regulation of floral organ abscission in Arabidopsis thaliana. *Proc Natl Acad Sci USA.*, *105*. https://doi.org/10.1073/pnas.0805539105

Clough, S. J., & Bent, A. F. (1998). Floral dip: a simplified method for Agrobacterium-mediated transformation of Arabidopsis thaliana. *The Plant Journal*, *16*(6), 735-743.

Crick, J., Corrigan, L., Belcram, K., Khan, M., Dawson, J. W., Adroher, B., Li, S., Hepworth, S. R., & Pautot, V. (2022). Floral organ abscission in Arabidopsis requires the combined activities of three TALE homeodomain transcription factors. *J Exp Bot*, *73*(18), 6150-6169. https://doi.org/10.1093/jxb/erac255

Dubiella, U., Seybold, H., Durian, G., Komander, E., Lassig, R., Witte, C. P., Schulze, W. X., & Romeis, T. (2013). Calcium-dependent protein kinase/NADPH oxidase activation circuit is required for rapid defense signal propagation. *Proc Natl Acad Sci U S A*, *110*(21), 8744-8749. https://doi.org/10.1073/pnas.1221294110

694 Dünser, K., Gupta, S., Herger, A., Feraru, M. I., Ringli, C., & Kleine-Vehn, J. (2019). Extracellular matrix
695 sensing by FERONIA and Leucine-Rich Repeat Extensins controls vacuolar expansion during
696 cellular elongation in Arabidopsis thaliana. *The EMBO journal*, *38*(7), e100353.
697 https://doi.org/10.15252/embj.2018100353
698 Earley, K. W., Haag, J. R., Pontes, O., Opper, K., Juehne, T., Song, K., & Pikaard, C. S. (2006). Gateway-
699 compatible vectors for plant functional genomics and proteomics. *Plant J*, *45*(4), 616-629.
700 https://doi.org/10.1111/j.1365-313X.2005.02617.x
701 Felix, G., Duran, J. D., Volko, S., & Boller, T. (1999). Plants have a sensitive perception system for the
702 most conserved domain of bacterial flagellin. *The Plant Journal*, *18*(3), 265-276.
703 https://onlinelibrary.wiley.com/doi/full/10.1046/j.1365-
704 313X.1999.00265.x?sid=nlm%3Apubmed
705 Feng, W., Kita, D., Peaucelle, A., Cartwright, H. N., Doan, V., Duan, Q., Liu, M. C., Maman, J., Steinhorst,
706 L., Schmitz-Thom, I., Yvon, R., Kudla, J., Wu, H. M., Cheung, A. Y., & Dinneny, J. R. (2018). The
707 FERONIA Receptor Kinase Maintains Cell-Wall Integrity during Salt Stress through Ca(2+)
708 Signaling. *Curr Biol*, *28*(5), 666-675.e665. https://doi.org/10.1016/j.cub.2018.01.023

709 Frerigmann, H., Pislewska-Bednarek, M., Sanchez-Vallet, A., Molina, A., Glawischnig, E., Gigolashvili, T.,
710 & Bednarek, P. (2016). Regulation of Pathogen-Triggered Tryptophan Metabolism in
711 Arabidopsis thaliana by MYB Transcription Factors and Indole Glucosinolate Conversion
712 Products. *Mol Plant*, *9*(5), 682-695. https://doi.org/10.1016/j.molp.2016.01.006
713 Geiger, D., Scherzer, S., Mumm, P., Marten, I., Ache, P., Matschi, S., Liese, A., Wellmann, C., Al-Rasheid,
714 K., & Grill, E. (2010). Guard cell anion channel SLAC1 is regulated by CDPK protein kinases with
715 distinct Ca2+ affinities. *Proceedings of the National Academy of Sciences*, *107*(17), 8023-8028.
716 Gómez-Gómez, L., Felix, G., & Boller, T. (1999). A single locus determines sensitivity to bacterial flagellin
717 in Arabidopsis thaliana. *Plant J*, *18*(3), 277-284. https://doi.org/10.1046/j.1365-
718 313x.1999.00451.x
719 Grini, P. E., Thorstensen, T., Alm, V., Vizcay-Barrena, G., Windju, S. S., Jorstad, T. S., Wilson, Z. A., &
720 Aalen, R. B. (2009). The ASH1 HOMOLOG 2 (ASHH2) histone H3 methyltransferase is required
721 for ovule and anther development in Arabidopsis. *PLoS One*, *4*(11), e7817.
722 https://doi.org/10.1371/journal.pone.0007817
723 Gronnier, J., Franck, C. M., Stegmann, M., DeFalco, T. A., Abarca, A., von Arx, M., Dünser, K., Lin, W.,
724 Yang, Z., Kleine-Vehn, J., Ringli, C., & Zipfel, C. (2022). Regulation of immune receptor kinase
725 plasma membrane nanoscale organization by a plant peptide hormone and its receptors. *Elife*,
726 *11*. https://doi.org/10.7554/eLife.74162
727 He, P., Shan, L., Lin, N. C., Martin, G. B., Kemmerling, B., Nurnberger, T., & Sheen, J. (2006). Specific
728 bacterial suppressors of MAMP signaling upstream of MAPKKK in Arabidopsis innate immunity.
729 *Cell*, *125*(3), 563-575. https://doi.org/10.1016/j.cell.2006.02.047
730 Hou, S., Wang, X., Chen, D., Yang, X., Wang, M., Turrà, D., Di Pietro, A., and Zhang, W. (2014). The
731 secreted peptide PIP1 amplifies immunity through Receptor-Like Kinase 7. PLoS Pathog 10:
732 e1004331.
733 Huffaker, A., Pearce, G., & Ryan, C. A. (2006). An endogenous peptide signal in Arabidopsis activates
734 components of the innate immune response. *Proc Natl Acad Sci U S A*, *103*(26), 10098-10103.
735 https://doi.org/10.1073/pnas.0603727103
736 Kadota, Y., Shirasu, K., & Zipfel, C. (2015). Regulation of the NADPH Oxidase RBOHD During Plant
737 Immunity. *Plant and Cell Physiology*, *56*(8), 1472-1480. https://doi.org/10.1093/pcp/pcv063
738 Kadota, Y., Sklenar, J., Derbyshire, P., Stransfeld, L., Asai, S., Ntoukakis, V., Jones, J. D., Shirasu, K.,
739 Menke, F., Jones, A., & Zipfel, C. (2014). Direct regulation of the NADPH oxidase RBOHD by the
740 PRR-associated kinase BIK1 during plant immunity. *Mol Cell*, *54*(1), 43-55.
741 https://doi.org/10.1016/j.molcel.2014.02.021
742 Keinath, N. F., Waadt, R., Brugman, R., Schroeder, J. I., Grossmann, G., Schumacher, K., & Krebs, M.
743 (2015). Live Cell Imaging with R-GECO1 Sheds Light on flg22- and Chitin-Induced Transient

[Ca(2+)]cyt Patterns in Arabidopsis. *Mol Plant*, *8*(8), 1188-1200. https://doi.org/10.1016/j.molp.2015.05.006

Kissoudis, C., Sunarti, S., van de Wiel, C., Visser, R. G., van der Linden, C. G., & Bai, Y. (2016). Responses to combined abiotic and biotic stress in tomato are governed by stress intensity and resistance mechanism. *J Exp Bot*, *67*(17), 5119-5132. https://doi.org/10.1093/jxb/erw285

Knight, H., Trewavas, A. J., & Knight, M. R. (1997). Calcium signalling in Arabidopsis thaliana responding to drought and salinity. *Plant J*, *12*(5), 1067-1078. https://doi.org/10.1046/j.1365-313x.1997.12051067.x

Knight, M. R., Campbell, A. K., Smith, S. M., & Trewavas, A. J. (1991). Transgenic plant aequorin reports the effects of touch and cold-shock and elicitors on cytoplasmic calcium. *Nature*, *352*(6335), 524-526. https://doi.org/10.1038/352524a0

Krebs, M., & Schumacher, K. (2013). Live cell imaging of cytoplasmic and nuclear Ca2+ dynamics in Arabidopsis roots. *Cold Spring Harbor Protocols*, *2013*(8), pdb. prot073031.

Kudla, J., Becker, D., Grill, E., Hedrich, R., Hippler, M., Kummer, U., Parniske, M., Romeis, T., & Schumacher, K. (2018). Advances and current challenges in calcium signaling. *New Phytol*, *218*(2), 414-431. https://doi.org/10.1111/nph.14966

Kumpf, R. P., Shi, C. L., Larrieu, A., Sto, I. M., Butenko, M. A., Peret, B., Riiser, E. S., Bennett, M. J., & Aalen, R. B. (2013). Floral organ abscission peptide IDA and its HAE/HSL2 receptors control cell separation during lateral root emergence. *Proc Natl Acad Sci U S A*, *110*(13), 5235-5240. https://doi.org/10.1073/pnas.1210835110

Kärkönen, A., & Kuchitsu, K. (2015). Reactive oxygen species in cell wall metabolism and development in plants. *Phytochemistry*, *112*, 22-32. https://doi.org/https://doi.org/10.1016/j.phytochem.2014.09.016

Ladwig, F., Dahlke, R. I., Stuhrwohldt, N., Hartmann, J., Harter, K., & Sauter, M. (2015). Phytosulfokine Regulates Growth in Arabidopsis through a Response Module at the Plasma Membrane That Includes CYCLIC NUCLEOTIDE-GATED CHANNEL17, H+-ATPase, and BAK1. *Plant Cell*, *27*(6), 1718-1729. https://doi.org/10.1105/tpc.15.00306

Lee, Y., Yoon, T. H., Lee, J., Jeon, S. Y., Lee, J. H., Lee, M. K., Chen, H., Yun, J., Oh, S. Y., Wen, X., Cho, H. K., Mang, H., & Kwak, J. M. (2018). A Lignin Molecular Brace Controls Precision Processing of Cell Walls Critical for Surface Integrity in Arabidopsis. *Cell*, *173*(6), 1468-1480.e1469. https://doi.org/10.1016/j.cell.2018.03.060

Li, L., Li, M., Yu, L., Zhou, Z., Liang, X., Liu, Z., Cai, G., Gao, L., Zhang, X., Wang, Y., Chen, S., & Zhou, J. M. (2014). The FLS2-associated kinase BIK1 directly phosphorylates the NADPH oxidase RbohD to control plant immunity. *Cell Host Microbe*, *15*(3), 329-338. https://doi.org/10.1016/j.chom.2014.02.009

Luna, E., Pastor, V., Robert, J., Flors, V., Mauch-Mani, B., & Ton, J. (2011). Callose deposition: a multifaceted plant defense response. *Mol Plant Microbe Interact*, *24*(2), 183-193. https://doi.org/10.1094/mpmi-07-10-0149

Ma, Y., Walker, R. K., Zhao, Y., & Berkowitz, G. A. (2012). Linking ligand perception by PEPR pattern recognition receptors to cytosolic Ca2+ elevation and downstream immune signaling in plants. *Proc Natl Acad Sci U S A*, *109*(48), 19852-19857. https://doi.org/10.1073/pnas.1205448109

Matsubayashi, Y. (2011). Post-translational modifications in secreted peptide hormones in plants. *Plant Cell Physiol*, *52*(1), 5-13. https://doi.org/10.1093/pcp/pcq169

McKenna, J. F., Rolfe, D. J., Webb, S. E. D., Tolmie, A. F., Botchway, S. W., Martin-Fernandez, M. L., Hawes, C., & Runions, J. (2019). The cell wall regulates dynamics and size of plasma-membrane nanodomains in Arabidopsis. *Proc Natl Acad Sci U S A*, *116*(26), 12857-12862. https://doi.org/10.1073/pnas.1819077116

Meng, X., Zhou, J., Tang, J., Li, B., de Oliveira, M. V., Chai, J., He, P., & Shan, L. (2016). Ligand-Induced Receptor-like Kinase Complex Regulates Floral Organ Abscission in Arabidopsis. *Cell Rep*, *14*(6), 1330-1338. https://doi.org/10.1016/j.celrep.2016.01.023

794 Meng, X., Zhou, J., Tang, J., Li, B., de Oliveira, M. V. V., Chai, J., He, P., & Shan, L. (2016). Ligand-Induced
795 Receptor-like Kinase Complex Regulates Floral Organ Abscission in Arabidopsis. *Cell reports*,
796 *14*(6), 1330-1338. https://doi.org/10.1016/j.celrep.2016.01.023
797 Monshausen, G. B., Messerli, M. A., & Gilroy, S. (2008). Imaging of the Yellow Cameleon 3.6 indicator
798 reveals that elevations in cytosolic Ca2+ follow oscillating increases in growth in root hairs of
799 Arabidopsis. *Plant Physiol*, *147*(4), 1690-1698. https://doi.org/10.1104/pp.108.123638
800 Niederhuth, C., Patharkar, O. R., & Walker, J. (2013). Transcriptional profiling of the Arabidopsis
801 abscission mutant hae hsl2 by RNA-Seq. *BMC Genomics*, *14*(1), 37.
802 http://www.biomedcentral.com/1471-2164/14/37
803 Olsson, V., Joos, L., Zhu, S., Gevaert, K., Butenko, M. A., & De Smet, I. (2018). Look Closely, the Beautiful
804 May Be Small: Precursor-Derived Peptides in Plants. *Annu Rev Plant Biol*.
805 https://doi.org/10.1146/annurev-arplant-042817-040413
806 Patharkar, O. R., Gassmann, W., & Walker, J. C. (2017). Leaf shedding as an anti-bacterial defense in
807 Arabidopsis cauline leaves. *PLoS Genet*, *13*(12), e1007132.
808 https://doi.org/10.1371/journal.pgen.1007132
809 Patharkar, O. R., & Walker, J. C. (2015). Floral organ abscission is regulated by a positive feedback loop.
810 *Proc Natl Acad Sci U S A*, *112*(9), 2906-2911. https://doi.org/10.1073/pnas.1423595112
811 Patharkar, O. R., & Walker, J. C. (2016). Core Mechanisms Regulating Developmentally Timed and
812 Environmentally Triggered Abscission. *Plant Physiol*, *172*(1), 510-520.
813 https://doi.org/10.1104/pp.16.01004
814 Poncini, L., Wyrsch, I., Dénervaud Tendon, V., Vorley, T., Boller, T., Geldner, N., Métraux, J. P., &
815 Lehmann, S. (2017). In roots of Arabidopsis thaliana, the damage-associated molecular pattern
816 AtPep1 is a stronger elicitor of immune signalling than flg22 or the chitin heptamer. *PLoS One*,
817 *12*(10), e0185808. https://doi.org/10.1371/journal.pone.0185808
818 Qi, Z., Verma, R., Gehring, C., Yamaguchi, Y., Zhao, Y., Ryan, C. A., & Berkowitz, G. A. (2010). Ca2+
819 signaling by plant Arabidopsis thaliana Pep peptides depends on AtPepR1, a receptor with
820 guanylyl cyclase activity, and cGMP-activated Ca2+ channels. *Proc Natl Acad Sci U S A*, *107*(49),
821 21193-21198. https://doi.org/10.1073/pnas.1000191107
822 Ranf, S., Eschen-Lippold, L., Pecher, P., Lee, J., & Scheel, D. (2011). Interplay between calcium signalling
823 and early signalling elements during defence responses to microbe- or damage-associated
824 molecular patterns. *Plant J*, *68*(1), 100-113. https://doi.org/10.1111/j.1365-
825 313X.2011.04671.x
826 Ranf, S., Grimmer, J., Poschl, Y., Pecher, P., Chinchilla, D., Scheel, D., & Lee, J. (2012). Defense-related
827 calcium signaling mutants uncovered via a quantitative high-throughput screen in Arabidopsis
828 thaliana. *Mol Plant*, *5*(1), 115-130. https://doi.org/10.1093/mp/ssr064
829 Robatzek, S., Chinchilla, D., & Boller, T. (2006). Ligand-induced endocytosis of the pattern recognition
830 receptor FLS2 in Arabidopsis. *Genes Dev*, *20*(5), 537-542. https://doi.org/10.1101/gad.366506
831 Roberts, J. A., Whitelaw, C. A., Gonzalez-Carranza, Z. H., & McManus, M. T. (2000). Cell Separation
832 Processes in Plants- Models, Mechanisms and Manipulation. *Annals of Botany*, *86*, 223-235.
833 Roman, A. O., Jimenez-Sandoval, P., Augustin, S., Broyart, C., Hothorn, L. A., & Santiago, J. (2022). HSL1
834 and BAM1/2 impact epidermal cell development by sensing distinct signaling peptides. *Nat*
835 *Commun*, *13*(1), 876. https://doi.org/10.1038/s41467-022-28558-4

836 Rzemieniewski, J., Leicher, H., Lee, H. K., Broyart, C., Nayem, S., Wiese, C., Maroschek, J., Camgöz, Z.,
837 Lalun, V. O., Djordjevic, M. A., Vlot, A. C., Hückelhoven, R., Santiago, J., & Stegmann, M. (2022).
838 Phytocytokine signaling integrates cell surface immunity and nitrogen limitation. *bioRxiv*,
839 2022.2012.2020.521212. https://doi.org/10.1101/2022.12.20.521212

840 Sanders, D., Brownlee, C., & Harper, J. F. (1999). Communicating with calcium. *Plant Cell*, *11*(4), 691-
841 706. https://doi.org/10.1105/tpc.11.4.691

Santiago, J., Brandt, B., Wildhagen, M., Hohmann, U., Hothorn, L. A., & Butenko, M. A. (2016). Mechanistic insight into a peptide hormone signaling complex mediating floral organ abscission. *Elife.*, *5*. https://doi.org/10.7554/eLife.15075

Scherzer, S., Maierhofer, T., Al-Rasheid, K. A. S., Geiger, D., & Hedrich, R. (2012). Multiple calcium-dependent kinases modulate ABA-activated guard cell anion channels. *Mol Plant*, *5*(6), 1409-1412. https://doi.org/10.1093/mp/sss084

Schindelin, J., Arganda-Carreras, I., Frise, E., Kaynig, V., Longair, M., Pietzsch, T., Preibisch, S., Rueden, C., Saalfeld, S., Schmid, B., Tinevez, J.-Y., White, D. J., Hartenstein, V., Eliceiri, K., Tomancak, P., & Cardona, A. (2012). Fiji: an open-source platform for biological-image analysis. *Nat Methods*, *9*(7), 676-682. https://doi.org/10.1038/nmeth.2019

Shi, C.-L., von Wangenheim, D., Herrmann, U., Wildhagen, M., Kulik, I., Kopf, A., Ishida, T., Olsson, V., Anker, M. K., Albert, M., Butenko, M. A., Felix, G., Sawa, S., Claassen, M., Friml, J., & Aalen, R. B. (2018). The dynamics of root cap sloughing in Arabidopsis is regulated by peptide signalling. *Nat Plants*, *4*(8), 596-604. https://doi.org/10.1038/s41477-018-0212-z

Smakowska-Luzan, E., Mott, G. A., Parys, K., Stegmann, M., Howton, T. C., Layeghifard, M., Neuhold, J., Lehner, A., Kong, J., Grunwald, K., Weinberger, N., Satbhai, S. B., Mayer, D., Busch, W., Madalinski, M., Stolt-Bergner, P., Provart, N. J., Mukhtar, M. S., Zipfel, C., . . . Belkhadir, Y. (2018). An extracellular network of Arabidopsis leucine-rich repeat receptor kinases. *Nature*, *553*(7688), 342-346. https://doi.org/10.1038/nature25184

Somssich, M., Bleckmann, A., & Simon, R. (2016). Shared and distinct functions of the pseudokinase CORYNE (CRN) in shoot and root stem cell maintenance of Arabidopsis. *J Exp Bot*, *67*(16), 4901-4915. https://doi.org/10.1093/jxb/erw207

Steinhorst, L., & Kudla, J. (2013). Calcium and reactive oxygen species rule the waves of signaling. *Plant Physiol*, *163*(2), 471-485. https://doi.org/10.1104/pp.113.222950

Stenvik, G. E., Tandstad, N. M., Guo, Y., Shi, C. L., Kristiansen, W., & Holmgren, A. (2008). The EPIP peptide of INFLORESCENCE DEFICIENT IN ABSCISSION is sufficient to induce abscission in Arabidopsis through the receptor-like kinases HAESA and HAESA-LIKE2. *Plant Cell.*, *20*. https://doi.org/10.1105/tpc.108.059139

Sto, I. M., Orr, R. J., Fooyontphanich, K., Jin, X., Knutsen, J. M., Fischer, U., Tranbarger, T. J., Nordal, I., & Aalen, R. B. (2015). Conservation of the abscission signaling peptide IDA during Angiosperm evolution: withstanding genome duplications and gain and loss of the receptors HAE/HSL2. *Front Plant Sci*, *6*, 931. https://doi.org/10.3389/fpls.2015.00931

Taylor, I., & Walker, J. C. (2018). Transcriptomic evidence for distinct mechanisms underlying abscission deficiency in the Arabidopsis mutants haesa/haesa-like 2 and nevershed. *BMC Res Notes*, *11*(1), 754. https://doi.org/10.1186/s13104-018-3864-x

Torres, M. A., & Dangl, J. L. (2005). Functions of the respiratory burst oxidase in biotic interactions, abiotic stress and development. *Curr Opin Plant Biol*, *8*(4), 397-403. https://doi.org/10.1016/j.pbi.2005.05.014

Vie, A. K., Najafi, J., Liu, B., Winge, P., Butenko, M. A., Hornslien, K. S., Kumpf, R., Aalen, R. B., Bones, A. M., & Brembu, T. (2015). The IDA/IDA-LIKE and PIP/PIP-LIKE gene families in Arabidopsis: phylogenetic relationship, expression patterns, and transcriptional effect of the PIPL3 peptide. *Journal of Experimental Botany*, *66*(17), 5351-5365. https://doi.org/10.1093/jxb/erv285

Wang, Y., Li, X., Fan, B., Zhu, C., & Chen, Z. (2021). Regulation and Function of Defense-Related Callose Deposition in Plants. *Int J Mol Sci*, *22*(5). https://doi.org/10.3390/ijms22052393

Main figures - A dual function of the IDA peptide in regulating cell separation and modulating plant immunity at the molecular level

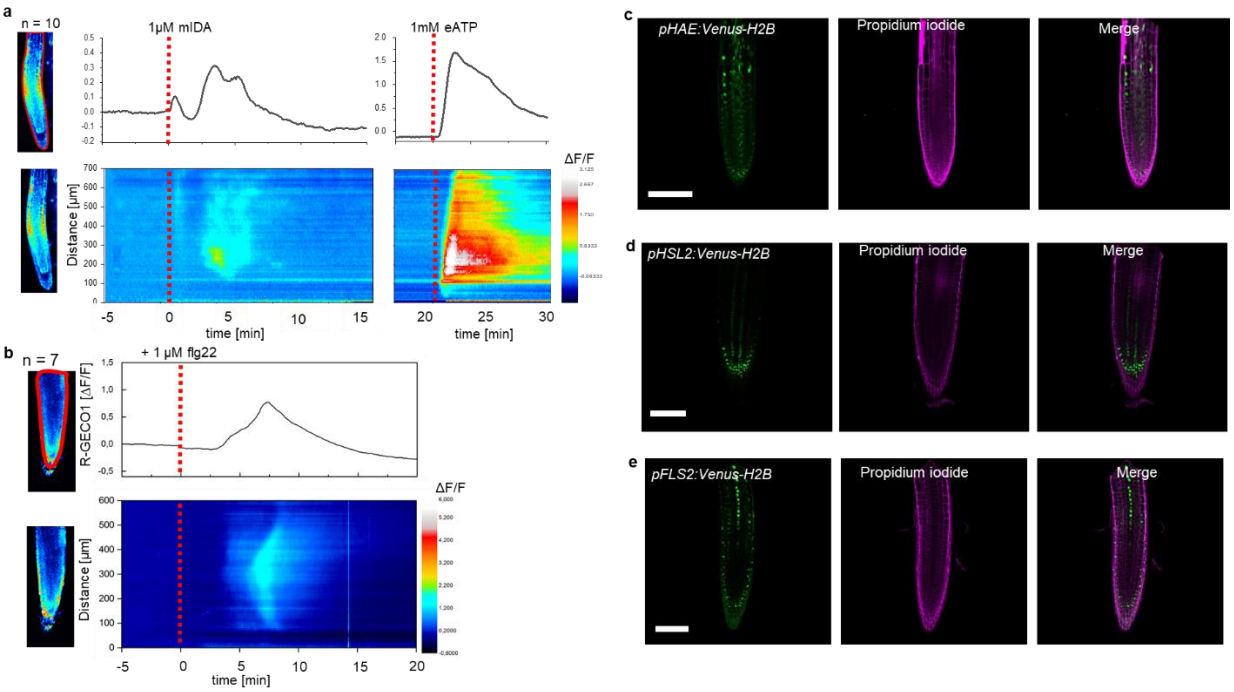

Fig. 1: mIDA-induced $[Ca^{2+}]_{cyt}$ release in Arabidopsis roots correlates with *pHAE* and *pHSL2* activity

a, Normalized R-GECO1 fluorescence intensities (ΔF/F) were measured from regions of interest (ROI) (upper panel, outlined in red) in the meristematic and elongation zone of the root. Fluorescence intensities (ΔF/F) over time of the whole root represented in a heat map (lower panel). Shown are cytosolic calcium concentration ($[Ca^{2+}]_{cyt}$) dynamics in the ROI in response to 1 µM mIDA over time. (see also Movie 1). Red lines at 5 minutes (min) indicates application of mIDA peptide or application of eATP at 22 min. Representative response from 10 roots (Sup Fig. 2). The increase in $[Ca^{2+}]_{cyt}$ response propagates through the roots as two waves. **b,** For comparison; Normalized R-GECO1 fluorescence intensities (ΔF/F) measured from regions of interest (ROI) (outlined in red, upper panel) in response to 1µM flg22 over time. Fluorescence intensities (ΔF/F) over time of the whole root represented in a heat map (lower panel). Red line at 0 min (min) indicates application of flg22 peptide. Representative response from 7 roots (Sup Fig. 3). The increase in $[Ca^{2+}]_{cyt}$ response propagates through the roots as a single wave seen as normalized R-GECO1 fluorescence intensities (ΔF/F) shown as a heat map (see also movie 2). **c,d,e**, Expression of the receptors **c**, *pHAE:Venus-H2B* **d**, *pHSL2:Venus-H2B* and **e**, *pFLS2:Venus-H2B* in 7 days-old roots. Representative pictures of n = 8. Scale bar = 50 µm, single plane image, magenta = propidium iodide stain.

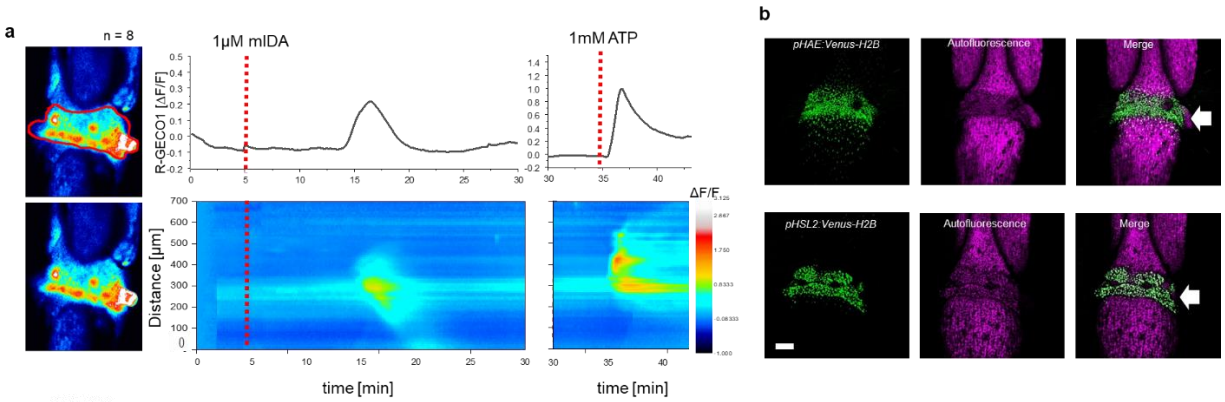

Fig. 2 : mIDA-induced $[Ca^{2+}]_{cyt}$ release in Arabidopsis abscission zones.

a, Normalized R-GECO1 fluorescence intensities (ΔF/F) were measured from regions of interest (ROI) (outlined in red) in floral abscission zone (AZ)s. Shown are cytosolic calcium concentration ($[Ca^{2+}]_{cyt}$) dynamics in the ROI in response to 1 µM mIDA over time (see also Movie 3). Representative response from 8 flowers (Sup. Fig 6). Red lines at 5 minutes (min) indicates application of mIDA peptide or application of eATP at 35 min (for AZs), respectively. The increase in $[Ca^{2+}]_{cyt}$ response propagates through the AZ as a single wave. **b**, Expression of *pHAE:Venus-H2B* and *pHSL2:Venus-H2B* in flowers at position 6 (See Sup Fig. 5a for positions) (arrowhead indicates AZ). Representative pictures of n = 8, scale bar = 100 µm, maximum intensity projections of z-stacks.

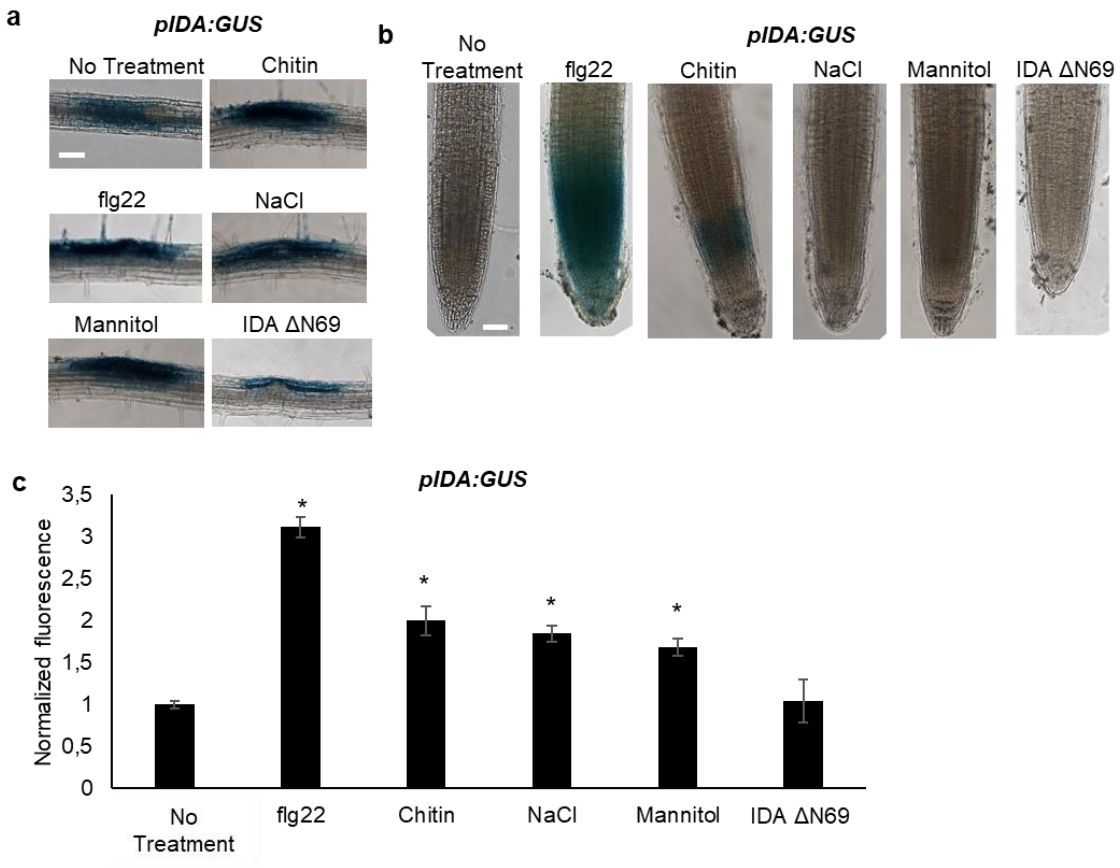

919

920 Fig. 3: *IDA* is induced by biotic and abiotic stress

921 Representative pictures of *pIDA:GUS* expression after 12 h treatment with 1 µM flg22, chitin, NaCl,
922 Mannitol and 1 µM IDAΔN69 in **a,** cells surrounding emerging lateral roots, and **b,** in the main root . **c**,
923 Normalized emitted fluorescence of fluorochrome 4-methyl umbelliferone (4-MU) in 7 days-old
924 seedlings after 12 h treatment with 1 µM flg22, chitin, NaCl, Mannitol and 1 µM of the inactive IDA
925 peptide, IDAΔN69. Normalized to 1 on No Treatment sample. Controls were not subjected to any stimuli
926 (No treatment). n = 6, experiment repeated 3 times. * = significantly different from the non-treated (No
927 treatment) sample ($p < 0.05$, student t-test, two tailed). Controls were not subjected to any stimuli (No
928 treatment). **a,b**, Representative picture of n = 10, experiment repeated 3 times, scale bar = 50 µm.

929

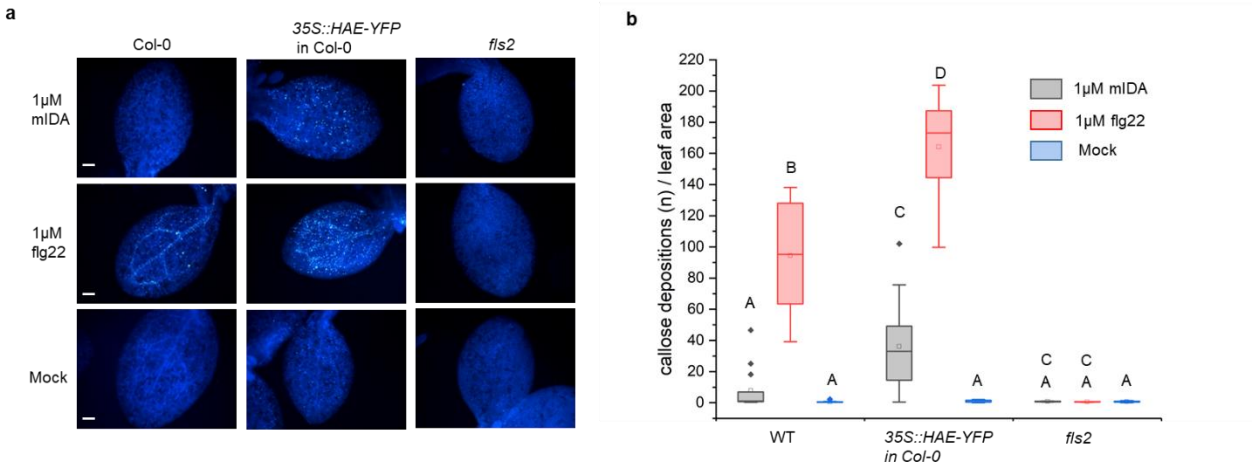

930

931 **Fig. 4: mIDA induce callose deposition in Arabidopsis cotelydons expressing 35S::HAE-YFP**

932 Callose deposition in Col-0 WT, 35S:HAE in Col-0 and *fls2* treated with water (mock treatment), 1 µM
933 mIDA or 1uM flg22. **a**, Callose deposition could be observed in cotyledons of eight day old Col-0 WT and
934 *35S:HAE in* seedlings treated with 1 µM flg22, and to a smaller extend in 35S:HAE treated with 1uM
935 mIDA. No callose deposition could be detected in the *fls2* mutant. Representative images of 9-12
936 seedlings per genotype. Scale bar 500 µm. **b**, Total callose depositions for the different genotypes
937 treated with water (mock treatment), 1 µM mIDA or 1 µM flg22. Statistically significant difference at ($p < 0,05$). N = 9-12

939

940

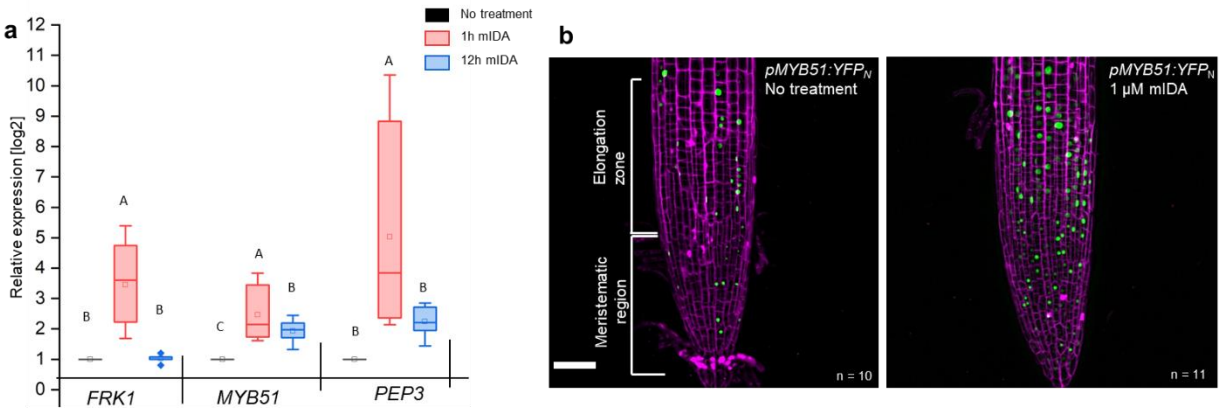

941

942 **Fig. 5: mIDA induced transcription of defense-associated marker genes**

943 **a**, Transcripts of *FRK1*, *MYB51*, and *PEP3* in WT Col-0 seedlings exposed to 1 µM mIDA for 1 h (red) and
944 to 1 µM mIDA for 12 h (blue) compared to untreated tissue (black). RNA levels were measured by RT-
945 qPCR analysis. *ACTIN* was used to normalize mRNA levels Figure represent three biological replicates
946 with four technical replicates. Statistical analyses was performed comparing induction times of
947 individual genes using one-way ANOVA and post-hoc Tukey's test ($p < 0.05$). **b**, *pMYB51:YFP$_N$* expression
948 is enhanced in roots after 7 h exposure to 1 µM mIDA peptide compared to untreated roots (control),
949 scale bar = 50 µm, maximum intensity projections of z-stacks, magenta = propidium iodide stain.

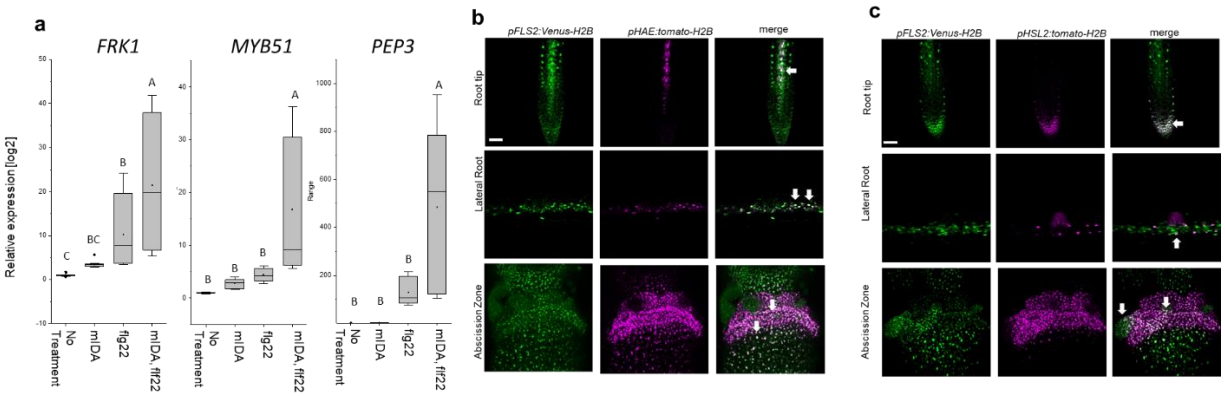

Fig. 6: mIDA and flg22 co-treatment extremely enhances the transcription of defense-associated marker genes

a, RT-qPCR data showing transcription of *FRK1*, *MYB51*, and *PEP3* in Col-0 WT seedlings exposed to 1 µM mIDA, 1 µM flg22 or a combination of 1 µM mIDA and 1 µM flg22 for 1 h compared to untreated seedlings (No treatment control). *ACTIN* was used to normalize mRNA levels. Figure represent three biological replicates with four technical replicates. Statistical analyses comparing No Treatment to peptide treated samples was performed using one-way ANOVA and post-hoc Tukey's test ($p < 0.05$). **b,** Microscopic analysis of 7-days-old *pFLS2:Venus-H2B pHAE:Tomato-H2B* expressing plants of root tip (upper panel) and lateral root (middle panel) of 7 days old plants, and flowers at position 6 (lower panel). Fluorescent nuclei representing co-expression of the Venus and Tomato marker could be observed in cells surrounding emerging LRs, in the stele of the root, as well as in the abscission zone. **c,** Microscopic analysis of 7-days-old *pFLS2:Venus-H2B pHSL2:Tomato-H2B* expressing plants of root tip (upper panel) and lateral root (middle panel) of 7 days old plants, and flowers at position 6 (lower panel). Fluorescent nuclei representing co-expression of the Venus and Tomato marker could be observed in the root tip, in cells surrounding emerging LRs, as well as in the abscission zone. Root pictures scale bar = 50 µm, single plane image. Abscission zone images= maximum intensity projections of z-stacks. Scale = 50µm.

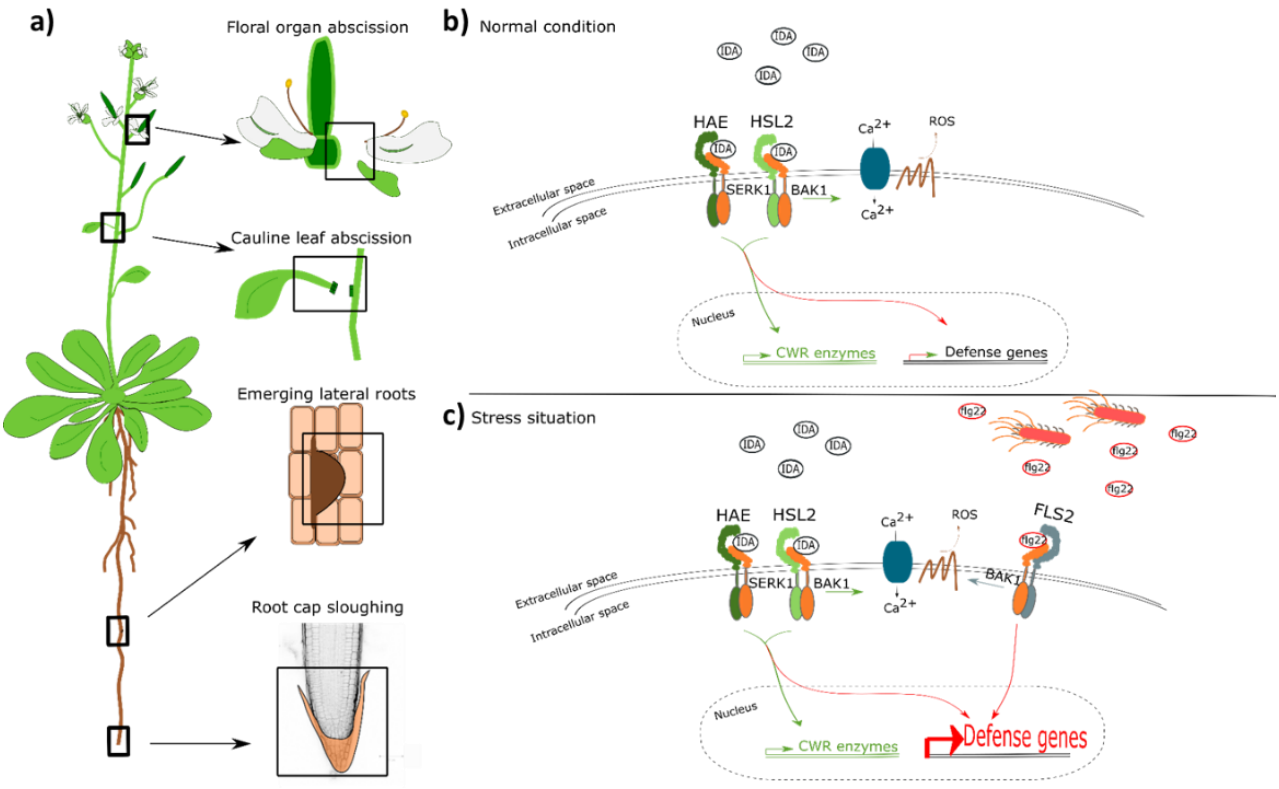

970

971 **Fig. 7: IDA regulates cell separation processes, but is also involved in major transcription of defense**
972 **genes upon pathogen attack.**

973 **a,** IDA and the IDL peptides control cell separation processes during plant development and in response
974 to abiotic and biotic stress (Butenko et al. 2003; Patharkar and Walker 2016; Patharkar et al. 2017; Shi
975 et al. 2018). Tissue undergoing cell separation includes floral organ abscission, cauline leaf abscission,
976 emerging of lateral roots and root cap sloughing. **b**, During normal conditions, IDA control floral organ
977 abscission and emergence of lateral roots by relaying a signal through receptor complexes including
978 HAE, HSL2, SERK1 and BAK1 to modulate the expression of cell wall remodeling (CWR) genes as well as
979 moderately expression of defense genes. IDA activates a receptor dependent production of ROS and an
980 increase in $[Ca^{2+}]_{cyt}$. **b,** Upon stress, such as pathogen attack, the activation of HAE and HSL2 acts in
981 addition to activation of defense related receptors, such as FLS2, to enhance the expression of defense
982 related genes significantly. This ensure optimal protection of cells undergoing cell separation, which
983 may be major entry routes during a pathogen attack.

984

985

Supplementary figures - A dual function of the IDA peptide in regulating cell separation and modulating plant immunity at the molecular level

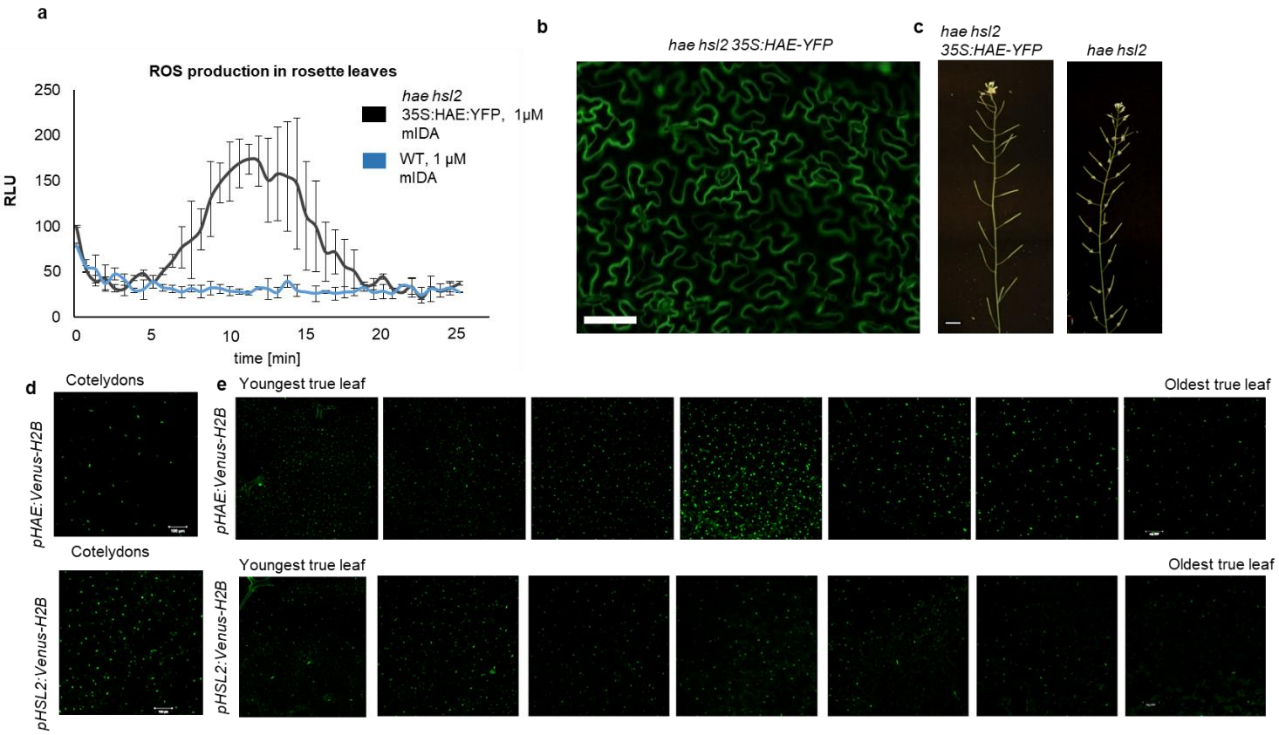

Sup Fig. 1: IDA induces ROS production in Arabidopsis

a, ROS production detected by the luminol-based assay was monitored over time as RLU. ROS production from *hae hsl2* leaf disks expressing *35S:HAE-YFP* in response to 1 µM mIDA (black) and in WT control (blue). **b**, Fluorescent image of *hae hsl2* rosette leaves expressing *35S:HAE:YFP*. Signal is detected in the plasma membrane of cells in the epidermal layer. Representative picture. Scale bar = 50 µm. **c,** *35S:HAE-YFP* complements the *hae hsl2* mutant abscission phenotype of observed. Scale = 1 cm. **d,e,** Microscopic analysis of *pHAE:Venus-H2B* (upper panel) and *pHSL2-Venus-H2B* (lower panel) in **d,** cotelydons of 7 days old seedlings and in **e,** rosette leaves of a 22 days old Arabidopsis plant containing 7 true leaves. Expression in each leaf is shown from youngest (left) to oldest (right). Scale = 100 µm

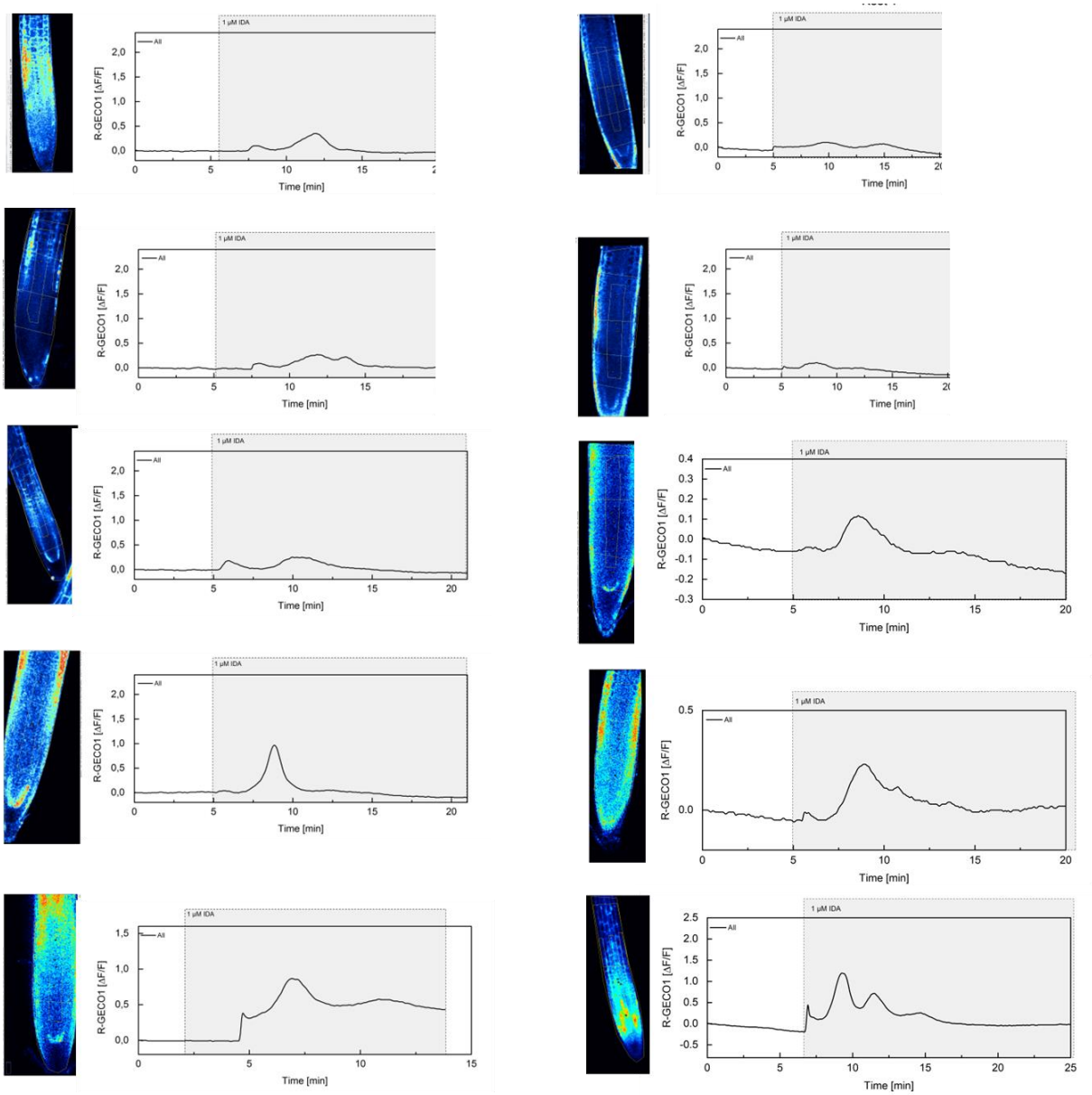

Sup Fig. 2: mIDA-induced $[Ca^{2+}]_{cyt}$ release in Arabidopsis roots

Shown are cytosolic calcium concentration ($[Ca^{2+}]_{cyt}$) dynamics in the ROI in response to 1 µM mIDA over time. Normalized R-GECO1 fluorescence intensities (ΔF/F) were measured from a region of interest (ROI) containing the meristematic and elongation zone of the root.

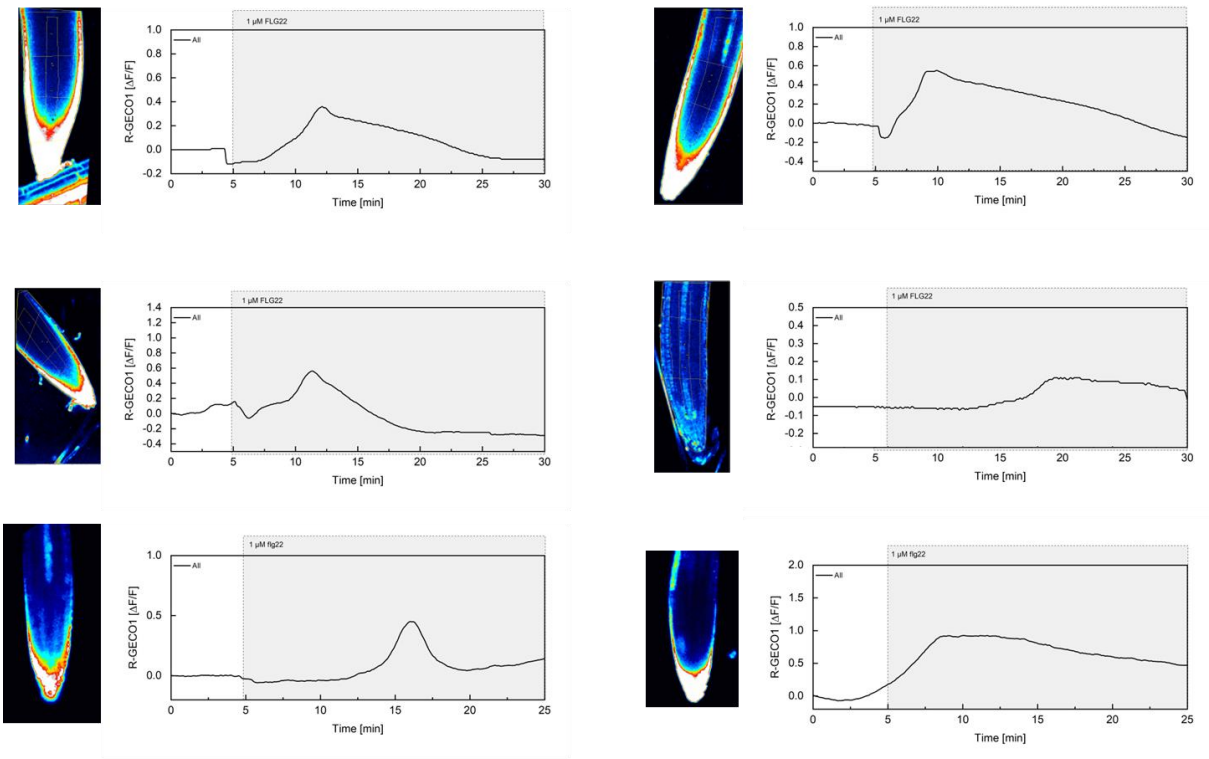

Sup Fig. 3: flg22-induced $[Ca^{2+}]_{cyt}$ release in Arabidopsis roots

Shown are cytosolic calcium concentration ($[Ca^{2+}]_{cyt}$) dynamics in the ROI in response to 1 µM flg22 over time. Normalized R-GECO1 fluorescence intensities (ΔF/F) were measured from a region of interest (ROI) containing the meristematic and elongation zone of the root.

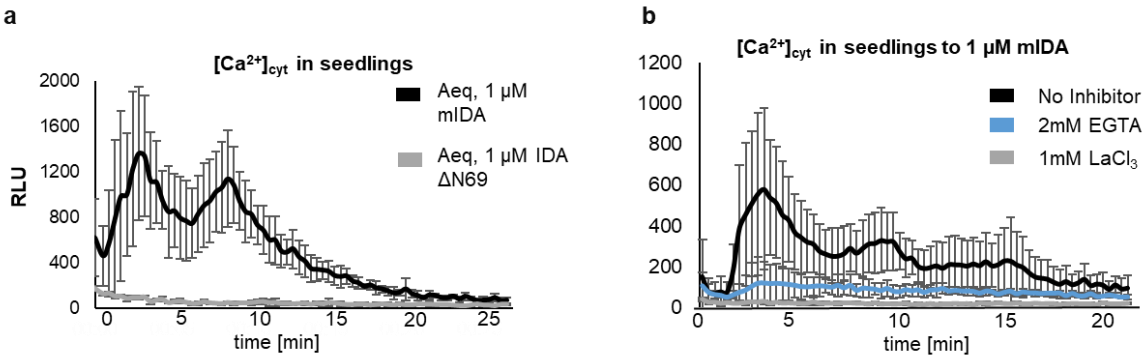

Sup Fig. 4 : The IDA triggered increase in $[Ca2+]_{cyt}$ is abolished in the presence of Ca^{2+} inhibitors

a, Increase in $[Ca^{2+}]_{cyt}$ in 7 days old seedlings expressing the cytosolic localized *Aequorin*-based luminescence Ca^{2+} sensor (*Aeq*) measured in relative light units (RLU) treated with 1 µM mIDA (black). No response is observed in *Aeq* seedlings treated with 1 µM IDAΔN69 (gray) or in *hae hsl2 Aeq* seedlings treated with 1 µM mIDA (blue). **b,** Increase in $[Ca^{2+}]_{cyt}$ in 7 days old seedlings expressing the cytosolic localized *Aequorin*-based luminescence Ca^{2+} sensor (*Aeq*) measured in relative light units (RLU) treated with 1 µM mIDA . No response is observed in *Aeq* seedlings treated with 1 mM EGTA (blue) or 1mM $LaCl_3$ (grey). Curves represent average of 3 independent experiments with 4-6 replicates in each experiment.

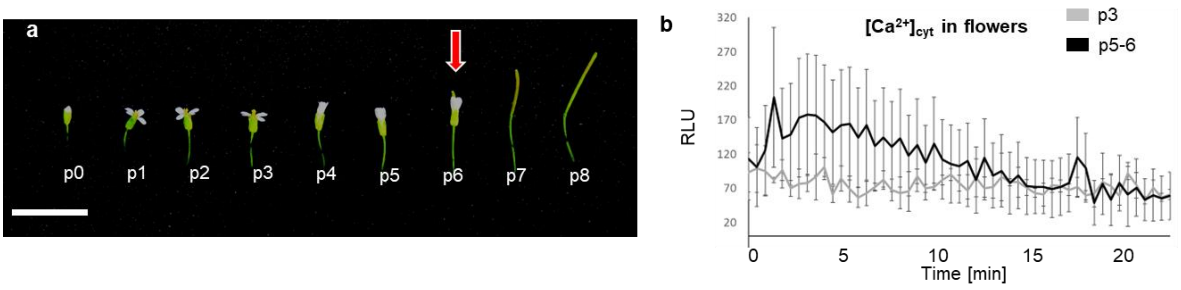

1032

1033 **Sup Fig. 5: mIDA induces a Ca^{2+} response in flowers**

1034 **a**, Arabidopsis flowers and siliques at different developmental stages. Flowers along the main
1035 inflorescence are counted from the first flower with visible white petals at the top of the inflorescence
1036 and is defined as p 1. Subsequently older flowers along the inflorescence (p0-p8). Cell wall remodeling
1037 in AZ cells, accompanied with a reduction in petal breakstrength (the force required to remove a petal
1038 from the receptacle) is initiated at p6 (red arrow). By p7 AZ cells have undergone cell separation and
1039 the floral organs have abscised. P=position **b**, Increase in $[Ca^{2+}]_{cyt}$ in flowers expressing the cytosolic
1040 localized *Aequorin*-based luminescence Ca^{2+} sensor (*Aeq*) measured in relative light units (RLU) treated
1041 with 1 µM mIDA. A $[Ca^{2+}]_{cyt}$ increase is observed in flowers where there is an initial weakening of the
1042 cell walls (p5-6) (black). No increase in luminescence was observed in *Aeq* expressing flowers of an
1043 earlier developmental stage (p3) (gray). Curves show representative measurements. Three
1044 independent experiments were performed with 4-6 replicates in each experiment.

1045

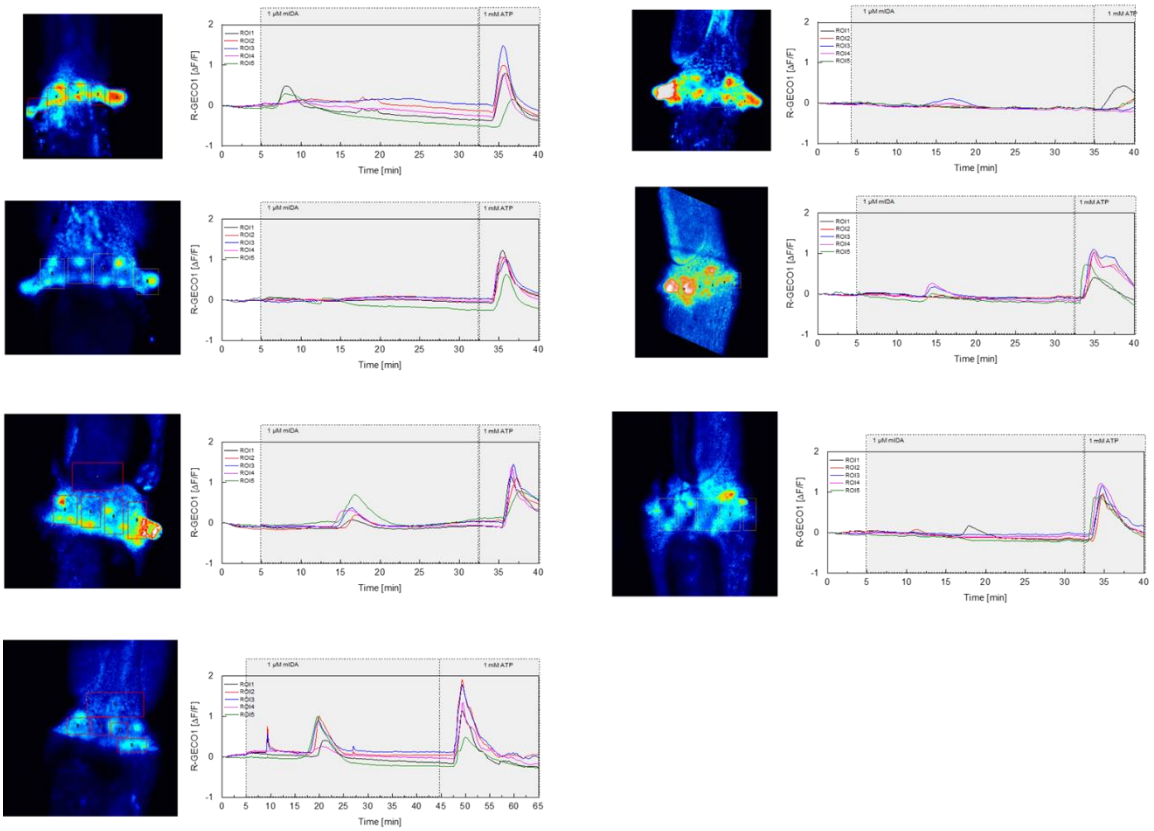

Sup Fig. 6: mIDA-induced $[Ca^{2+}]_{cyt}$ release in Arabidopsis abscission zones. Normalized R-GECO1 fluorescence intensities (ΔF/F) were measured from regions of interest (ROIs) in floral abscission zone (AZ)s. Shown are cytosolic calcium concentration ($[Ca^{2+}]_{cyt}$) dynamics in the ROI1-5 in response to 1 µM mIDA over time.

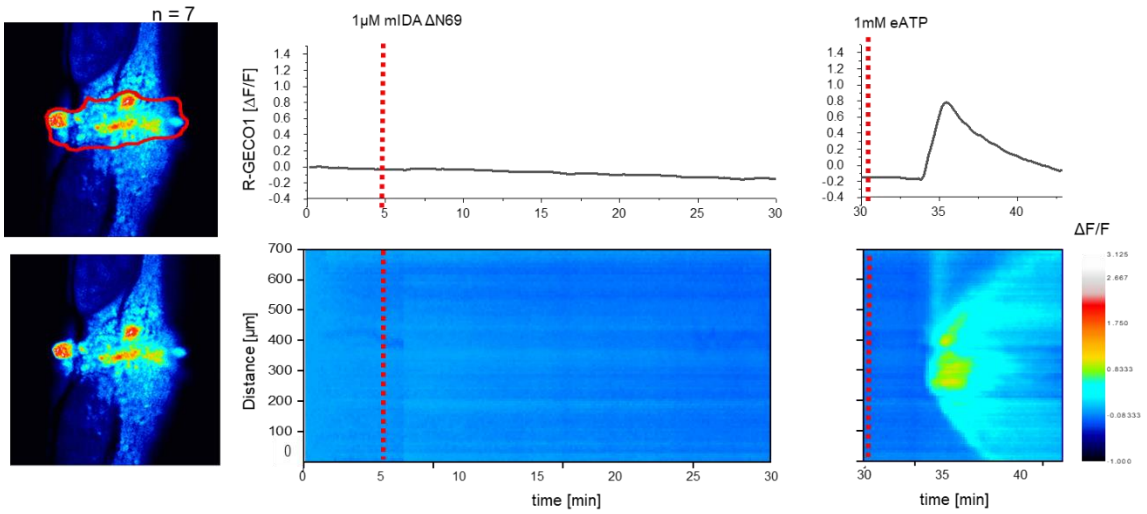

Sup Fig. 7 : mIDAΔN69 does not induce a $[Ca^{2+}]_{cyt}$ release in Arabidopsis abscission zones (AZ)

Normalized R-GECO1 fluorescence intensities (ΔF/F) were measured from regions of interest (ROI) (outlined in red) in the floral AZs. Shown are cytosolic calcium concentration ($[Ca^{2+}]_{cyt}$) dynamics in the ROI in response to application of 1 µM mIDAΔN69 or eATP over time. Red lines at 5 minutes (min) indicates application of mIDAΔN69 peptide or application of eATP at 30 min (see also Movie 4). Representative response from 10 flowers. The increase in $[Ca^{2+}]_{cyt}$ response to eATP propagates through the AZ as a single wave seen as normalized R-GECO1 fluorescence intensities (ΔF/F) shown as a heat map.

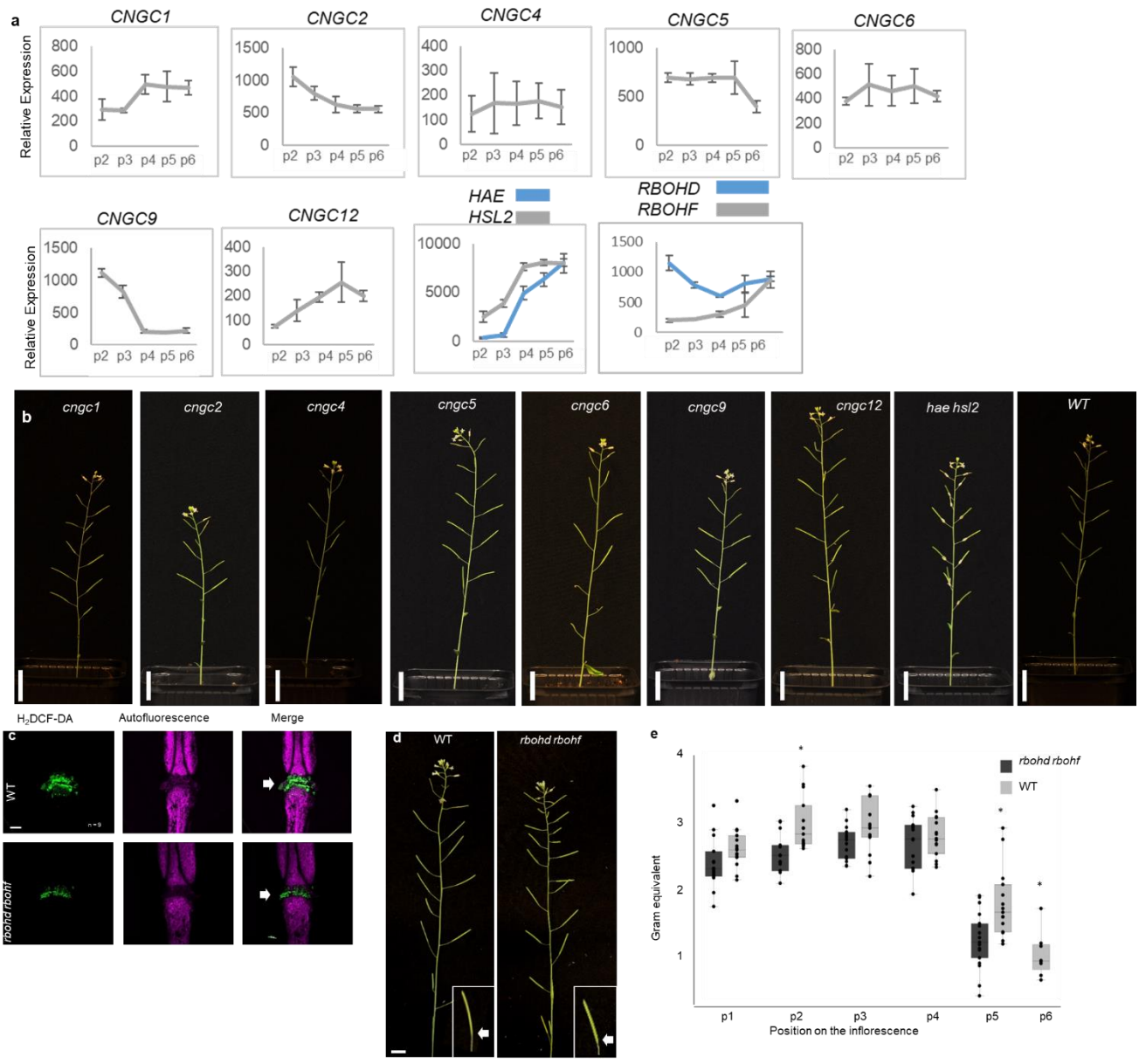

1065

1066 **Sup Fig. 8: Investigation of CNGCs and RBOHs in the abscission process**

1067 **a,** Relative expression of *CNGC1*, *CNGC2*, *CNGC4*, *CNGC5*, *CNGC6*, *CNGC9*, *CNGC12, RBOHD* and *RBOHF*
1068 in the floral organs during the onset of abscission (Cai and lashbrook 2008). X-axis represents the
1069 developmental stages of abscission where position 12 represent flowers where the stamen and petals
1070 are of the same length, position 13 represent flowers at anthesis, position 15 represent flowers with
1071 stigma extended above the anthers. Floral organ abscission occurs at position 15. Relative expression
1072 of *HAE* and *HSL2* added for comparison. Nomenclature for the abscission process and relative
1073 expression values taken from (Cai and Lashbrook 2008). **b**, No floral organ abscission phenotype is
1074 observed in the single *cngc* mutant plants compared to the *hae hsl2* mutant which retains the floral
1075 organ indefinitely. Scale bar = 2cm, 5 weeks old plants. **c**, ROS production in the AZ (white arrow head)
1076 detected by using the fluorescent dye H_2DCF-DA in WT and *rbohd rbohf* flowers at position 6 (See

Supplementary Fig. 5a for positions). Scale bar = 100 µm, maximum intensity projections of z-stacks. Representative pictures from 9 flowers. **d**, Representative pictures of WT and *rbohd rbohf* inflorescences, scale bar for inflorescences = 1 cm. **e**, Petal break strength (pBS) measurements of WT and the *rbohd rbohf* mutant at position 1-6 along the inflorescence. Force required to remove petals from the receptacle represented in gram equivalent. * = significantly different from WT at the given position ($p < 0.05$, student t-test, two tailed).

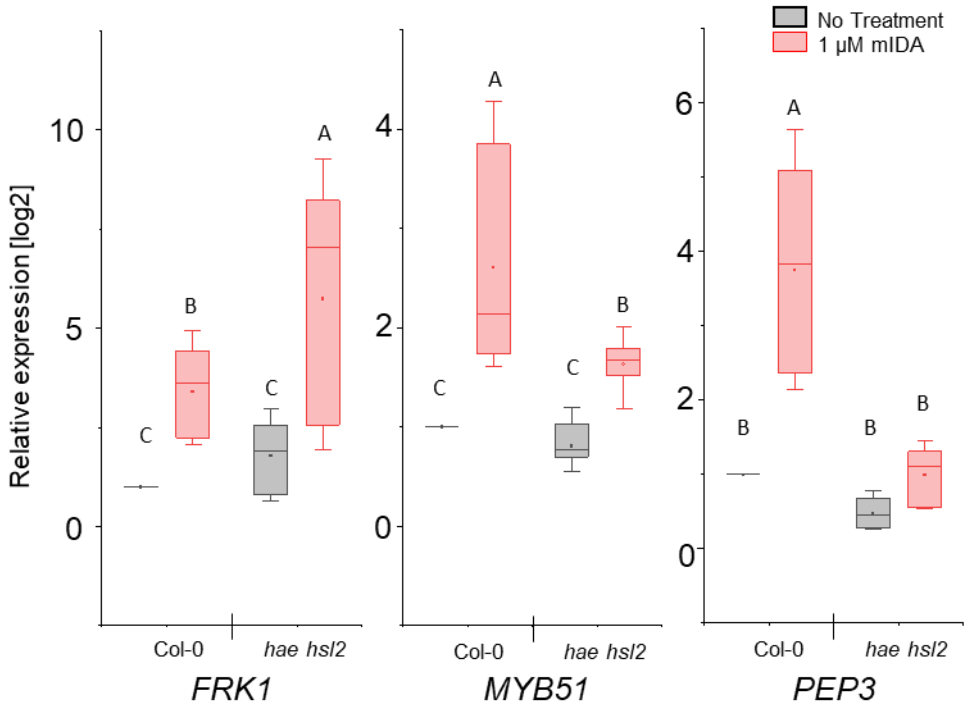

Sup Fig. 9: mIDA induced enhanced transcription of defense-associated marker genes is only partially dependent on the HAE and HSL2 receptors

RT-qPCR data showing transcription of *FRK1*, *MYB51*, and *PEP3* in Col-0 WT and *hae hsl2* seedlings exposed to 1 µM mIDA for 1 h compared to untreated seedlings (No treatment). *ACTIN* was used to normalize mRNA levels. Figure represent 3 biological replicates with 4 technical replicates. Statistical analyses was performed comparing samples within same gene, using two-way ANOVA and post-hoc Tukey's test ($p < 0.05$).

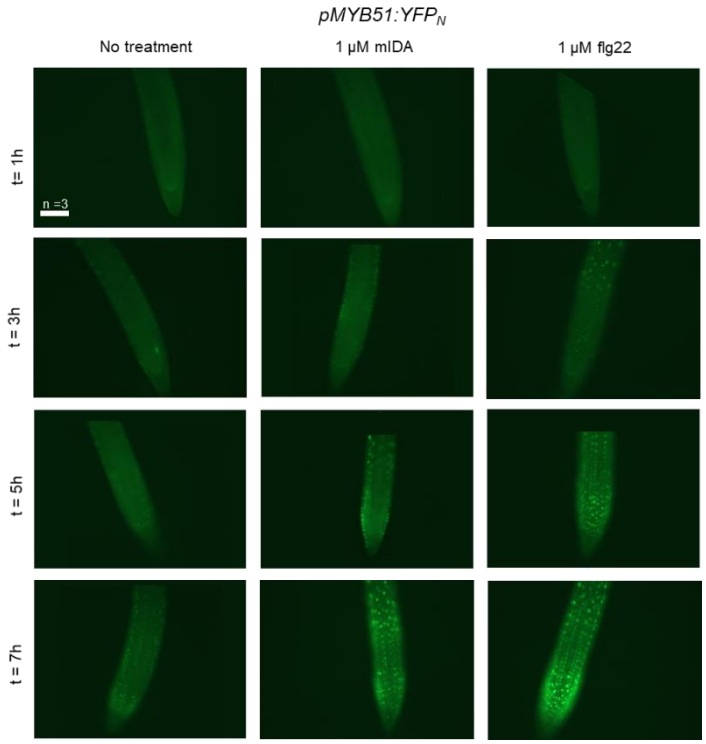

Sup Fig. 10: mIDA and flg22 induced expression of *pMYB51:YFP*

Representative microscopic pictures of 7-days-old *pMYB51:YFPN* roots from seedlings transferred to liquid medium with 1 µM flg22 or 1 µM mIDA for 1, 3, 5 and 7 h using a fluorescent microscope. Control seedlings were transferred to medium with no peptide and imaged in the same time frame. Fluorescent nuclei could be observed in a similar temporal pattern in roots subjected to mIDA and flg22. Scale bar = 100 µm, single plane images using a Zeiss Axioplan2 microscope with an AxioCam HRc, 20x air objective and a YFP filter (Excitation: 500/20, Beamsplitter: FT515, Emission: 535/50), no imaging processing was performed, t = time in h. n = 3, experiment repeated 3 times.

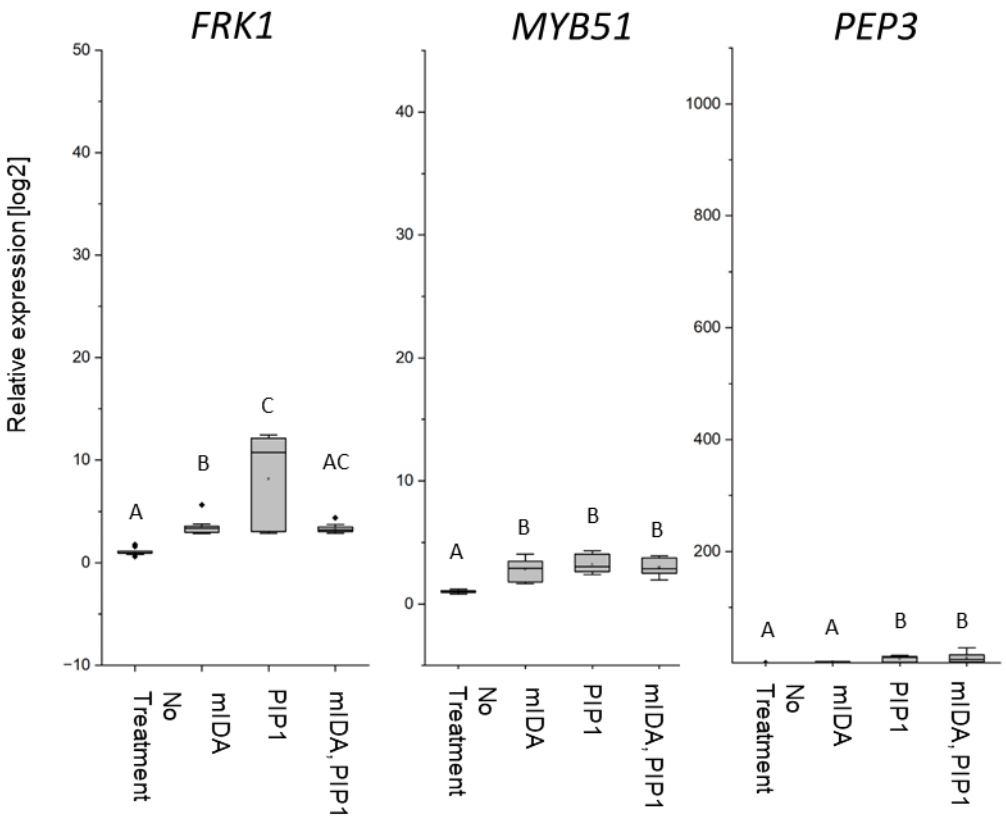

Sup Fig. 11 : mIDA and PIP1 co-treatment do not enhances transcription of defense-associated marker genes

RT-qPCR data showing transcription of *FRK1*, *MYB51*, and *PEP3* in Col-0 WT seedlings exposed to 1 µM mIDA, 1 µM PIP1 or a combination of 1 µM mIDA and 1 µM PIP1 for 1 h compared to untreated seedlings (No treatment control). *ACTIN* was used to normalize mRNA levels. Figure showing extended results from experiment shown in Fig 6. For comparison, No treatment and mIDA treated samples were included in the figure (same results presented in Fig 6). Scale on y axis was kept as in Fig 6. Figure represents 2-3 biological replicates with 4 technical replicates. Statistical analyses comparing the samples was performed using one-way ANOVA and post-hoc Tukey's test ($p < 0.05$).

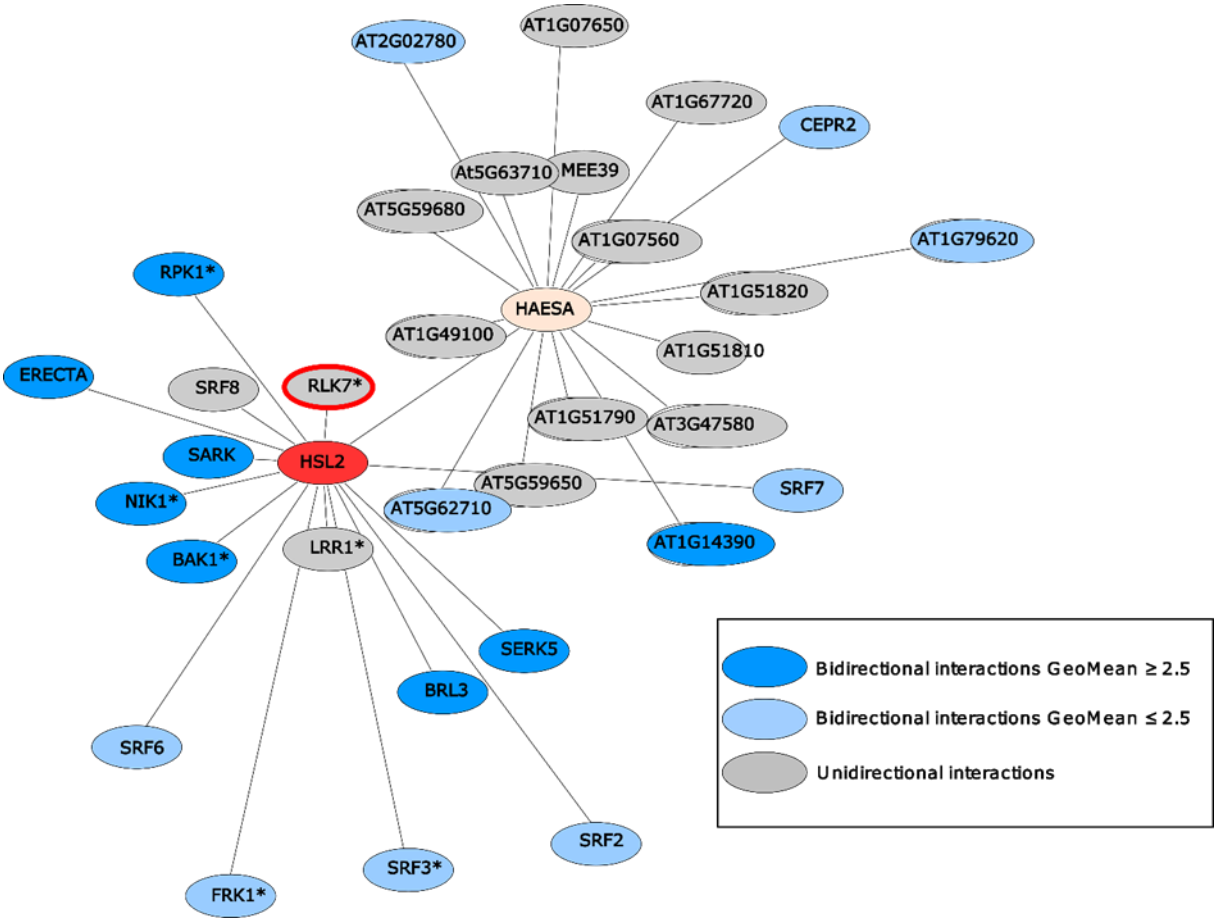

Sup Fig. 12: HAE (yellow) and HSL2 (red) display very distinct repertoire of immune and growth-related interacting LRR-RKs.

HEA and HSL2 specific interacting partners determined using a sensitized high-throughput extracellular domain interaction assay (Smakowska-Luzan et al,.2018). HSL2 and HAE show distinct interacting LRR-RKs where only HSL2 was found to interact with RLK7 (red halo). * indicates receptors known to play a function in biotic and/or abiotic responses in planta based on previous published work, dark blue nodes refer to bidirectional interactions with GeoMean ≥2.5, light blue nodes- refer to bidirectional interactions with GeoMean ≤2.5, and grey nodes refer to unidirectional interactions.

1127

1128

1129